Terahertz laser spectroscopy of the water dimer intermolecular vibrations. I. $(D_2O)_2$

L. B. Braly, J. D. Cruzan,[a] K. Liu,[b] R. S. Fellers,[c] and R. J. Saykally[d]
Department of Chemistry, University of California, Berkeley, California 94720

(Received 24 January 2000; accepted 6 March 2000)

Terahertz laser VRT spectra of the water dimer consisting of 731 transitions measured with an average precision of 2 MHz and involving four $(D_2O)_2$ intermolecular vibrations (one previously published) have been measured between 65 and 104 cm^{-1}. The precisely determined energy level patterns differ both qualitatively and quantitatively from the predictions of several dimer potentials tested, and reveal an ordering of the intermolecular vibrations which differs dramatically from that predicted by standard normal mode analysis. Strong coupling is indicated between the low barrier tunneling motions and the intermolecular vibrations as well as among different vibrations. Particularly, the 83 cm^{-1} (acceptor wag) and 90 cm^{-1} $(D_2O)_2$ (acceptor twist) vibrations interact through a Coriolis perturbation. These spectra provide the basis for our recent determination of the water pair potential. The corresponding data set for $(H_2O)_2$ is presented in an accompanying paper.
 [S0021-9606(00)00721-2]

I. INTRODUCTION

Recent work has shown that it is possible, in principle, to quantitatively determine the force field for liquid water and ice through the detailed study of small water clusers.[1–3] Analysis of the interaction energies of these clusters indicates that the major component is the pair potential, accounting for perhaps 70% of the binding energy.[4] Moreover, the principal constituent of the three-body, as well as the much smaller four- and higher-body terms is induction (polarization), which is already contained in the pair potential if the low-order multipole moments and polarizability are properly included. The pair potential thus accounts for most (>90%) of the cohesive energy of liquid and solid water, with the remainder due mostly to the three-body exchange forces. It is therefore necessary to begin with a rigorously accurate pair potential in order to properly describe liquid water and ice. Despite great effort, this crucial step eluded previous researchers.

The water pair potential can be accessed experimentally through indirect inversion of the infrared and terahertz VRT spectra of the water dimer, as has been accomplished for simpler cases such as Ar–H_2O,[5] Ar–NH_3,[6] and $(HCl)_2$,[7] and $(NH_3)_2$.[8] The intermolecular vibrations of such complexes sensitivily sample both the repulsive wall and the attractive well of an intermolecular potential surface (IPS), and the associated hydrogen bond rearrangement tunneling splittings rigorously constrain the detailed topology. While the computational effort required to extract the detailed IPS for a six-dimensional system like the water dimer is formidable, this has recently been accomplished.[3] In this and the accompanying paper, we present the results from our measurement and analysis of extensive terahertz VRT spectra of $(D_2O)_2$ and $(H_2O)_2$ that provided the basis for our recent determination of the IPS.[3]

A. Hydrogen bond rearrangement tunneling in the water dimer

It is apparent from microwave and infrared studies that the water dimer is a highly nonrigid, near prolate top molecule (Fig. 1) that undergoes several simultaneous tunneling motions within the molecular framework.[9,10] These motions lead to a complicated VRT spectrum. This is now a familiar behavior of weakly bound systems, as observed in a number of hydrogen bonded dimers including $(HCl)_2$ (Ref. 7) and $(NH_3)_2$.[11] In order to describe the VRT spectra, of such molecules, it is first essential to identify the permutation–inversion (PI) group and to classify the molecular energy levels. Dyke used the G_{16} group for the water dimer to successfully interpret his microwave spectra in a 1977 paper.[10] The following description is derived from the cumulative work of Dyke,[9,12] Hougen,[13] Coudert and Hougen,[14] and Pugliano *et al.*[15,16]

There are 16 equivalent structures of the water dimer that can be generated without breaking chemical bonds. Permutation of identical nuclei gives rise to eight equivalent structures. Inversion of these structures through the center of mass generates eight more configurations. The dimer tunnels along low-energy barrier pathways on the six-dimensional intermolecular potential energy surface (IPS) to access the different structures. If the equilibrium structure contains a plane of symmetry, as the available evidence strongly supports, then there are only eight unique minima on the six dimensional (6D) IPS.

The corresponding PI symmetry group (G_{16}), is used to explain the resulting splittings in the revibrational energy levels. G_{16} is isomorphic with the $D_{4h}(M)$ point group and

[a]Department of Chemistry, Harvard University, Cambridge, Massachusetts.
[b]Department of Chemistry, University of Southern California, Los Angeles, California.
[c]Lawrence Livermore National Laboratory, Livermore, California.
[d]Author to whom correspondence should be addressed.

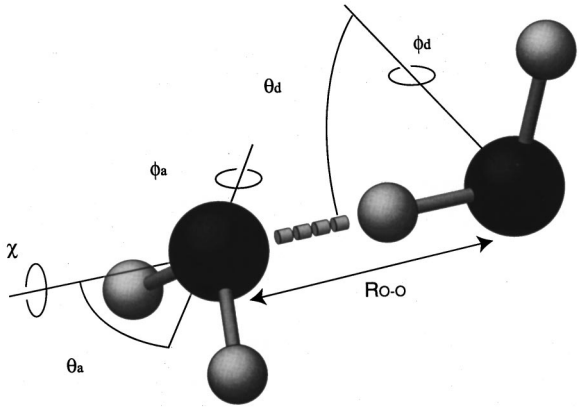

FIG. 1. The vibrationally averaged water dimer structure. $R_{O-O}=2.94$ Å, $\theta_a=41°$, $\phi_d=58°$, $\phi_a=90°$, $\phi_d=0°$, and $\chi=180°$. Structure calculated using DQMC on VRT(ASP-W) (Ref. 1).

is consistent with the observed VRT dynamics. The water dimer samples the eight distinct minima on the 6D IPS by tunneling via three low energy barrier pathways.[17,18] In the correlation diagram in Fig. 2, energy levels for $J=0$, $K_a=0$ and $J=1$, $K_a=0$ of the semirigid framework are labeled by vibrational symmetry A' and A'', respectively, corresponding to the C_s subgroup.

1. Acceptor switching (AS)

The acceptor switching (AS) rearrangement pathway (Fig. 3) has the lowest energy barrier, estimated to be 130 cm^{-1} on the IPS of Coker and Watts[14] and 157 cm^{-1} on the VRT(ASP-W) potential of Fellers *et al.*[3] This motion allows exchanges of the protons in the water molecule acting as the H-bond acceptor. The tunneling pathway beings with a flip of the acceptor monomer followed by a rotation of the donor monomer about its O–H bond. A 180° rotation of the complex about the O–O bond completes the pathway and returns the dimer to a permutationally distinct equivalent version. While the actual pathway includes three separate rotations within the dimer, the net effect is a C_2 rotation of the acceptor about its symmetry axis. Each rovibrational energy level of the semirigid water dimer is split into two by this tunneling motion. When this motion is included, the symmetry group becomes $C_{2v}(M)$, and the resulting energy levels are labeled A_1/B_1 and A_2/B_2 as shown in Fig. 2.

2. Interchange (I)

The next most feasible tunneling motion is labeled as interchange (I), in which the roles of the individual donor and acceptor water molecules are exchanged. The effect is to split each of the $C_{2v}(M)$ energy levels into three but by a much smaller degree than for acceptor switching tunneling. The VRT states are now labeled in the $G_{16}[D_{4h}(M)]$ molecular symmetry group as $A_1^+/E_1^+/B_1^+$ and $A_2^-/E_2^-/B_2^-$ for $J=0$ $K_a=0$. The $E(\pm)$ states are doubly degenerate. These two tunneling motions resolve all possible degeneracies in the water dimer eigenstates.

There are two possible pathways which produce this net effect, with the lowest barrier associated with the geared interchange $[I(g)]$ motion shown in Fig. 3. This motion begins

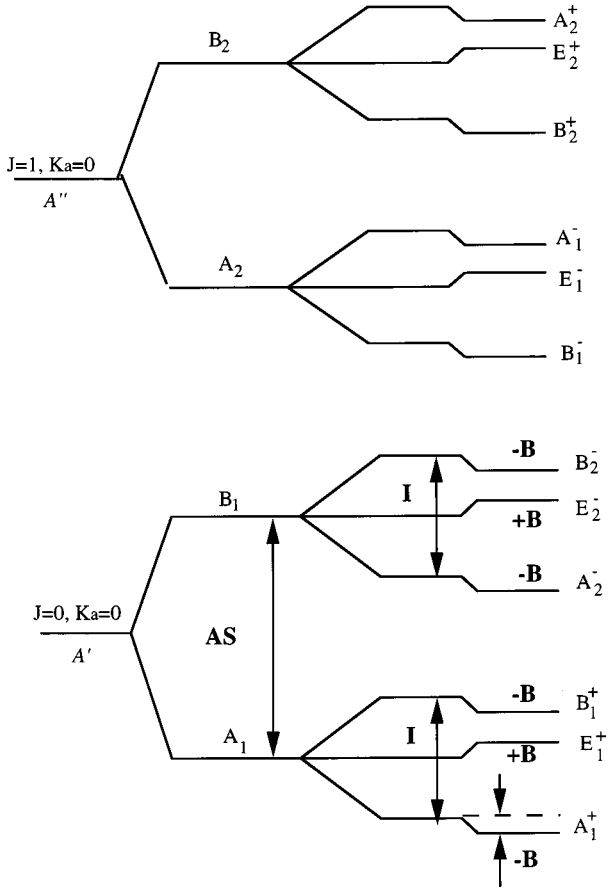

FIG. 2. Correlation diagram for the VRT levels of the water dimer in G_{16}. The bold print represents the three tunneling splittings or shift. The letters which are not in boldface are symmetry levels labeled using the G_{16} molecular symmetry group.

with a rotation of the acceptor monomer about its C_2 symmetry axis and a rotation of the donor in the θ_d angle to form the *trans*- transition state structure shown in Fig. 3. The pathway continues with rotation of the θ_a so that now the acceptor is the donor and a rotation of the donor about its C_2 axis such that it becomes the acceptor. The pathway is completed when the complex undergoes 180° end-over-end rotation. Recent calculations on the VRT(ASP-W) potential energy surface show that this pathway has a barrier of 207 cm^{-1} (Ref. 3) compared to the calculations by Coudert and Hougen[14] on the potential of Coker and Watts which estimates this barrier to be 800 cm^{-1}.

Coudert and Hougen[17] later identified the antigeared interchange $[I(ag)]$ pathway as contributing significantly in their fit of the available $(H_2O)_2$ data at the time to their local internal axis method (IAM) model. In this model, the effect of this tunneling manifests itself as a difference in the Interchange splitting of the A_1/B_1 states and the A_2/B_2 states. In the ground state, $K_a''=0$ energy levels, the total I of the A_1/B_1 states is

$$I=I(g)+I(ag)=22.6\,\text{GHz},$$

and in the A_2/B_2 states, it is

$$I=I(g)-I(ag)=19.5\,\text{GHz},$$

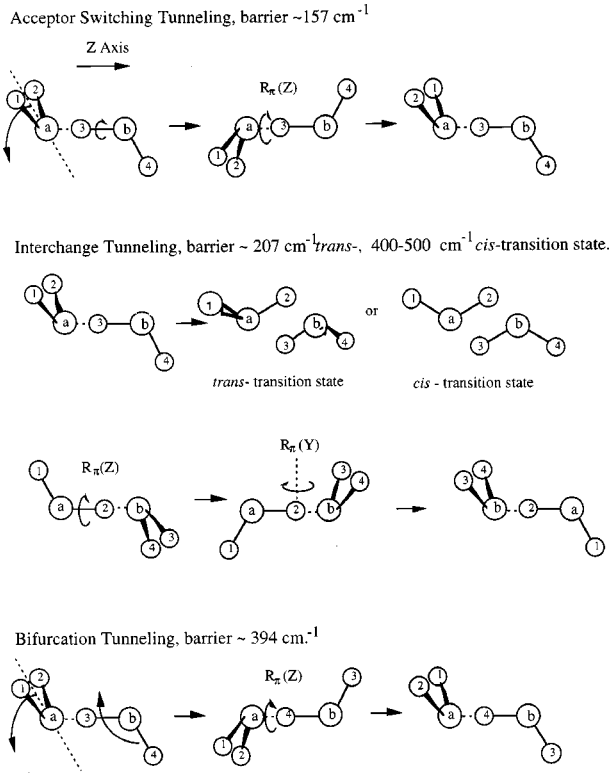

FIG. 3. The three tunneling pathways. These pathways (Ref. 18) have the lowest barriers. The interchange pathway includes the geared and antigeared versions of the tunneling motion with the geared motion having the lower barrier. Reported barrier heights are for VRT(ASP-W) (Ref. 1).

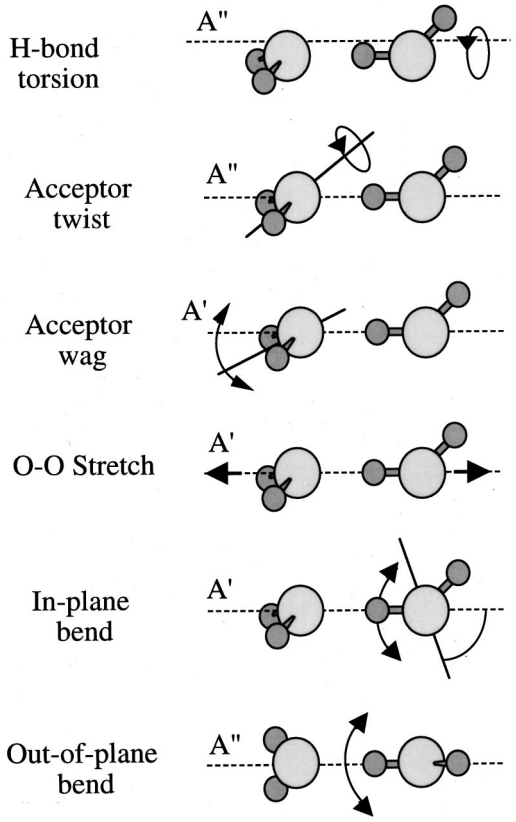

FIG. 4. The six normal mode intermolecular vibrations of the water dimer. These were determined and labeled in Ref. 19.

In their analysis, Coudert and Hougan determined that $I(g)$ is 21 GHz and $I(ag)$ is 1.6 GHz such that $I(ag)$ makes up $<5\%$ of the total interchange splitting in the ground state. No antigeared pathway was found on VRT(ASP-W). However, three slightly different *cis*-transition states were identified on VRT(ASP-W) also having geared pathways. These barrier heights in the range of 400–500 cm^{-1}, slightly higher than that of the *trans*-transition state.[3]

3. Bifurcation (B)

The final rearrangement identified is Bifurcation tunneling (B) wherein the H-bond donor permutes its protons (Fig. 3). The barrier to this motion is estimated to be about 1000 cm^{-1} in Ref. 14 and 394 cm^{-1} by VRT(ASP-W).[3] The result is a small shift of the rovibrational energy levels, but no further splitting occurs since all degeneracies are already resolved by the acceptor switching and interchange. The donor monomer moves into a ''bifurcated'' hydrogen bond transition state wherein each of its protons shares one half of the hydrogen bond.[18] The net effect is a C_2 rotation of the donor about its symmetry axis.

The projection of the molecular electric dipole moment along an axis fixed in space is invariant to permutation of identical nuclei changes sign under E^*. Therefore, this operator transforms like A_1^- in G_{16}. This leads to the overall selection rules $A_1^+ \leftrightarrow A_1^-$, $B_1^+ \leftrightarrow B_1^-$, $A_2^+ \leftrightarrow A_2^-$, $B_2^+ \leftrightarrow B_2^-$, $E^+ \leftrightarrow E^-$ (Ref. 10).

The fully deuterated dimer has 81 spin functions. The total wave function must be symmetric for bosons in the cases of both even and odd permutations of nuclei. The wave functions transform like A_1^+ or A_1^- in G_{16}. The nuclear spin weights are A_1^+/A_1^- (Ref. 21), B_1^+/B_1^- (Ref. 15), A_2^+/A_2^- (Ref. 3), B_2^+/B_2^- (Ref. 6), E^+/E^- (Ref. 18).

There are no missing transitions in the $(D_2O)_2$ spectra. The intensity of a transition will follow the nuclear spin weights if the linewidth is greater than the hyperfine splittings. This is the case for infrared and far infrared spectroscopies, but microwave spectroscopy has the capacity to resolve the hyperfine splittings.

B. The intermolecular vibrations

A normal mode analysis was performed by Reimer and Watts[19] on their RWK2[20] IPS. There are 12 normal modes for the water dimer; six correspond to intramolecular vibrations and six correspond to intermolecular vibrations. These six intermolecular modes are shown and labeled in Fig. 4 according to the Reimer and Watts scheme. The Reimer and Watts harmonic vibrational frequencies for $(H_2O)_2$ are given in Table I along with the anharmonic intermolecular vibrational frequencies determined from VRT(ASP-W)[1] for both $(H_2O)_2$ and $(D_2O)_2$.[2] It is well known that the actual intermolecular vibrations in very floppy hydrogen bonded clusters often occur at frequencies as low as half of the calculated harmonic values, and that the atomic motions are not as simple as those shown. They are more likely to be linear combinations of the normal modes. However, when discussing these vibrations, these normal vibration labels will be used and connections to them made whenever possible.

TABLE I. Predictions for the six intermolecular vibrational frequencies (cm^{-1}).

Vibration	Harmonic approx.[a] $(H_2O)_2$	VRT(ASP-W)II[b] $(H_2O)_2$	VRT(ASP-W)II[b] $(D_2O)_2$
H-bond torsion	141	90	69
Acceptor twist	147	119	78
Acceptor wag	155	105	80
O–O stretch	185	150	135
In-plane bend	342	142	115
Out-of-plane bend	632	na	na

[a]Harmonic approximation using RWK2 (Ref. 19).
[b]Results from the VRT(ASP-W)II (Ref. 3).

The lowest energy normal mode is the donor torsion (ν_{12}). This mode involves only the donor molecule with its free hydrogen rotating about the donor O–H bond (or the donor monomer symmetry axis, ϕ_d). It is labeled with A'' symmetry, because the motion is out of the plane of symmetry, as opposed to A' vibrations for which the motion is in the plane of symmetry.

The next two lowest vibrations are close in energy: the acceptor twist (ν_{11}) and the acceptor wag (ν_8). The acceptor twist (A'') allows the acceptor monomer to rotate about its C_2 axis by ϕ_a. The acceptor wag (A') involves rotation of the acceptor monomer in the θ_a coordinate. In other words, the motion is through the angle that is created between the acceptor C_2 axis and the molecular center-of-mass coordinate or the hydrogen bond.

The A' in-plane donor bend (ν_6) involves motion of the donor monomer C_2 axis with respect to the hydrogen bond, or θ_d. It is similar to the acceptor wag except that it directly strains the hydrogen bond, thus making it higher in energy. The out-of-plane donor bend (ν_{10}) is an A'' vibration which is characterized by a rotation about the dihedral angle (χ) that is measured between the C_2 axes of the monomers. This motion also strains the hydrogen bond and is similarly expected to occur at relatively high frequency.

The A' O–O stretch (ν_7), or hydrogen bond stretch, is the last of the intermolecular vibrations described here. As the name suggests it is the vibration along the center-of-mass coordinate or hydrogen bond. It is expected to have a weak spectrum due to the small change in the dipole moment. Analysis of the ground state centrifugal distortion constants predicts this vibration to occur near 150 cm^{-1}.[12,14]

II. EXPERIMENT

Terahertz laser spectroscopy is a direct absorption technique characterized by high sensitivity (ca. 1×10^{-6} minimum detectable fractional absorption) and high resolution (ca. 1×10^{-6} or 1 MHz) and currently operates in the frequency range 1–4.5 THz (30–150 cm^{-1}). This technique is used to directly probe and characterize the weak bonds of van der Waals and hydrogen-bonded clusters and has been used in studies of water clusters as large as the hexamer.[21–24] The first study of the water dimer with this approach was reported by Busarow *et al.* in 1989.[25]

TABLE II. Terahertz laser list.

Freq./GHz	Freq./cm^{-1}	Gas
1626.6026	54.2576	CH_2F_2
1838.8393	61.3371	CH_3OH
1891.2743	63.0861	CH_2F_2
1987.7989	66.3058	CH_2DOH
2058.1418	68.6522	CH_3OD
2216.2634	73.9266	CH_2F_2
2252.0541	75.1204	CH_2DOH
2409.2932	80.3654	CH_2F_2
2447.9685	81.6554	CD_3OH
2522.7815	84.1509	CH_3OH
2546.495	84.9419	CH_2F_2
2633.8991	87.8574	$^{13}CH_3OH$
2714.7151	90.5531	$^{13}CH_3OH$
2742.946	91.4948	CH_2F_2
2907.0889	96.97	CH_3OD
3105.9368	103.6029	CH_3OH
3239.4614	108.0568	CH_3OH
3356.8304	111.9718	CH_3OD
3494.4413	116.562	$^{13}CH_3OH$
3690.7231	123.1093	N_2H_2

The Berkeley terahertz spectrometers have been described in detail elsewhere[26–28] and are similar to the instrument originally built in 1985 but with several modifications introduced in recent years to increase the spectral range and the concentration of large (>3) water clusters.[29–31] The water dimer is easily observed under these new conditions. What follows is a brief overview of the spectrometer and pulsed slit jet source with specifics on the far infrared laser gases (Table II) used to obtain the water dimer data discussed here.

The output from a line tunable CO_2 laser (operating power of 70–150 W) is used to longitudinally pump a line tunable far infrared (FIR) laser. The fixed frequency far in-

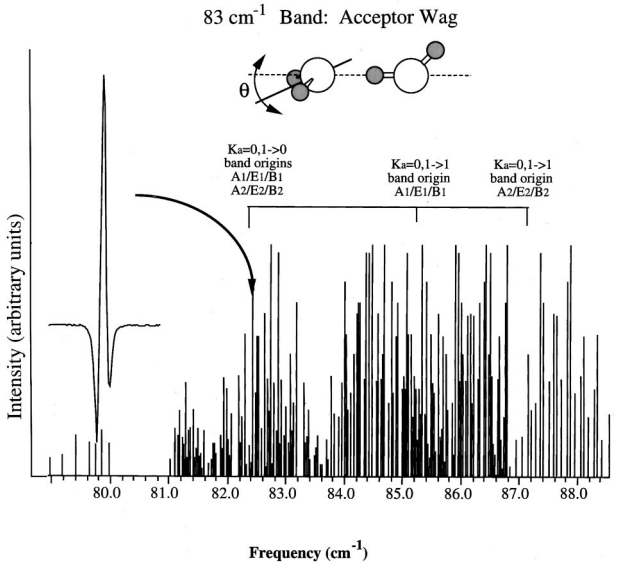

FIG. 5. 83 cm^{-1} $(D_2O)_2$ stick spectrum, acceptor wag (ν_8). Three hundred sixty-three *a*- and *c*-type transitions with $K_a=0\rightarrow0$, $0\rightarrow1$, $1\rightarrow0$, and $1\rightarrow1$ observed. Maximum signal-to-noise for *a*-type ~50:1 and for *c*-type ~100:1, linewidth ~2 MHz.

TABLE III. 83 cm^{-1} $(D_2O)_2$ band, acceptor wag (ν_8) transition frequencies (MHz). Residuals (observed–calculated) are in italics.

Transition		A_1^+, B_1^-	Obs–Calc		E^+, E^-	Obs–Calc		B_1^+, A_1^-	Obs–Calc
				$K_a = 0 \rightarrow 0$ *a*-type transitions					
$8_{08} \leftarrow 9_{09}$				E^-	2 377 482.7	*−1.8*			
$7_{07} \leftarrow 8_{08}$				E^+	2 388 845.2	*−2.9*	B_1^+	2 386 140.1	*−1.0*
$6_{06} \leftarrow 7_{07}$				E^-	2 400 163.8	*−0.7*	A_1^-	2 397 484.1	*−0.3*
$5_{05} \leftarrow 6_{06}$	A_1^+	2 413 992.7	*0.2*	E^+	2 411 430.4	*2.9*	B_1^+	2 408 772.0	*0.6*
$4_{04} \leftarrow 5_{05}$	B_1^-	2 425 178.7	*−0.5*	E^-	2 422 632.1	*−0.2*	A_1^-	2 419 997.1	*−0.4*
$3_{03} \leftarrow 4_{04}$				E^+	2 433 776.6	*2.2*	B_1^+	2 431 158.9	*1.5*
$2_{02} \leftarrow 3_{03}$				E^-	2 444 850.3	*−0.2*	A_1^-	2 442 245.4	*−2.1*
$1_{01} \leftarrow 2_{02}$	A_1^+	2 458 372.1	*0.7*	E^+	2 455 859.9	*2.0*	B_1^+	2 453 263.2	*−1.3*
$0_{00} \leftarrow 1_{01}$				E^-	2 466 794.7	*0.2*	A_1^-	2 464 203.9	*−2.0*
$1_{01} \leftarrow 0_{00}$	A_1^+	2 490 963.6	*−2.0*	E^+	2 488 450.9	*0.4*	B_1^+	2 485 863.8	*7.8*
$2_{02} \leftarrow 1_{01}$	B_1^-	2 501 652.4	*0.3*	E^-	2 499 167.7	*−1.1*	A_1^-	2 496 564.9	*1.2*
$3_{03} \leftarrow 2_{02}$	A_1^+	2 512 350.3	*1.0*	E^+	2 509 814.7	*0.7*	B_1^+	2 507 194.0	*0.0*
$4_{04} \leftarrow 3_{03}$	B_1^-	2 522 941.4	*3.4*	E^-	2 520 381.1	*−6.1*	A_1^-	2 517 748.7	*0.4*
$5_{05} \leftarrow 4_{04}$	A_1^+	2 533 456.3	*−3.1*	E^+	2 530 892.3	*2.5*	B_1^+	2 528 230.3	*1.4*
$6_{06} \leftarrow 5_{05}$	B_1^-	2 543 915.3	*0.0*	E^-	2 541 327.1	*3.2*	A_1^+	2 538 641.2	*2.7*
$7_{07} \leftarrow 6_{06}$	A_1^+	2 554 306.4	*−1.6*	E^+	2 552 693.8	*1.4*	B_1^+	2 548 979.7	*−0.9*
$8_{08} \leftarrow 7_{07}$	B_1^-	2 564 641.6	*1.2*	E^-	2 561 999.5	*0.5*	A_1^-	2 559 258.3	*−0.8*
$9_{09} \leftarrow 8_{08}$	A_1^+	2 574 916.0	*0.1*	E^+	2 572 250.5	*2.3*	B_1^+	2 569 479.7	*1.4*
$10_{010} \leftarrow 9_{09}$				E^-	2 582 444.6	*−1.0*	A_1^-	2 579 642.3	*−0.4*
Transition		A_2^+, B_2^-	Obs–Calc		E^+, E^-	Obs–Calc		B_2^+, A_2^-	Obs–Calc
$9_{09} \leftarrow 10_{010}$	B_2^-	2 364 286.6	*−2.0*	E^-	2 366 644.0	*−7.6*			
$8_{08} \leftarrow 9_{09}$	A_2^+	2 375 573.0	*−1.3*	E^+	2 377 935.1	*−1.8*			
$7_{07} \leftarrow 8_{08}$	$_2^-$	2 386 814.9	*−1.1*	E^-	2 389 174.8	*−4.9*			
$6_{06} \leftarrow 7_{07}$	$_2^+$	2 398 012.9	*−0.3*				B_2^+	2 402 467.3	*0.5*
$5_{05} \leftarrow 6_{06}$	B_2^-	2 409 166.3	*1.2*	E^-	2 411 533.2	*1.5*	A_2^-	2 413 615.7	*0.7*
$4_{04} \leftarrow 5_{05}$	A_2^+	2 420 271.2	*−0.1*	E^+	2 422 638.4	*−0.1*	B_2^+	2 424 710.1	*−5.3*
$3_{03} \leftarrow 4_{04}$	B_2^-	2 431 329.6	*−0.1*	E^-	2 433 696.6	*−1.5*	A_2^-	2 435 765.0	*−3.7*
$2_{02} \leftarrow 3_{03}$	A_2^+	2 442 338.6	*−2.3*	E^+	2 444 710.9	*0.2*			
$1_{01} \leftarrow 2_{02}$	B_2^-	2 453 305.7	*1.7*	E^-	2 455 673.1	*−2.0*	A_2^-	2 457 735.4	*0.5*
$0_{00} \leftarrow 1_{01}$				E^+	2 466 590.3	*0.3*	B_2^+	2 468 646.8	*−0.7*
$1_{01} \leftarrow 0_{00}$	B_2^-	2 485 897.2	*1.2*	E^-	2 488 267.3	*−0.5*	A_2^-	2 490 329.5	*0.7*
$2_{02} \leftarrow 1_{01}$	A_2^+	2 496 658.2	*0.2*	E^+	2 499 030.1	*1.1*	B_2^+	2 501 097.1	*1.6*
$3_{03} \leftarrow 2_{02}$	B_2^-	2 507 368.4	*0.7*	E^-	2 509 738.4	*0.7*	A_2^-	2 511 812.7	*1.6*
$4_{04} \leftarrow 3_{03}$	A_2^+	2 518 022.9	*−1.5*	E^+	2 520 390.6	*−2.8*	B_2^+	2 522 475.6	*1.7*
$5_{05} \leftarrow 4_{04}$	B_2^-	2 528 628.4	*1.2*	E^-	2 530 996.8	*0.9*	A_2^-	2 533 081.3	*−0.6*
$6_{06} \leftarrow 5_{05}$	A_2^+	2 539 173.3	*1.6*	E^+	2 541 542.0	*4.1*	B_2^+	2 543 636.2	*1.3*
$7_{07} \leftarrow 6_{06}$	B_2^-	2 549 663.1	*1.4*	E^-	2 552 025.9	*1.1*	A_2^-	2 554 135.1	*0.5*
$8_{08} \leftarrow 7_{07}$	A_2^+	2 560 094.0	*−0.3*	E^+	2 562 456.9	*3.3*	B_2^+	2 564 573.7	*−4.6*
$9_{09} \leftarrow 8_{08}$	B_2^-	2 570 467.5	*−1.1*	E^-	2 572 826.9	*3.6*	A_2^-	2 574 962.9	*−2.1*
$10_{010} \leftarrow 9_{09}$	A_2^+	2 580 785.9	*2.3*	E^+	2 583 135.7	*2.3*	B_2^+	2 585 296.4	*2.8*
Transition		A_1^+, B_1^-	Obs–Calc		E^+, E^-	Obs–Calc		B_1^+, A_1^-	Obs–Calc
				$K_a = 1 \rightarrow 1$ *a*-type transitions					
$4_{13} \leftarrow 5_{14}$	B_1^-	2 356 464.8	*0.8*	E^-	2 349 744.1	*0.2*			
$3_{12} \leftarrow 4_{13}$	A_1^+	2 367 399.4	*0.9*	E^+	2 360 644.3	*2.0*	B_1^+	2 354 484.6	*0.1*
$2_{11} \leftarrow 3_{12}$	B_1^-	2 378 321.8	*0.4*	E^-	2 371 539.1	*2.1*	A_1^-	2 365 352.3	*1.1*
$1_{10} \leftarrow 2_{11}$	A_1^+	2 389 226.1	*−5.6*	E^+	2 382 429.7	*0.2*			
$1_{10} \leftarrow 1_{11}$	A_1^+	2 411 026.6	*−2.3*				B_1^+	2 398 020.5	*−2.9*
$2_{11} \leftarrow 2_{12}$	B_1^-	2 411 066.4	*1.6*				A_1^-	2 398 094.0	*−0.3*
$3_{12} \leftarrow 3_{13}$	A_1^+	2 411 120.6	*1.9*				B_1^+	2 398 202.6	*1.7*
$4_{13} \leftarrow 4_{14}$	B_1^-	2 411 193.6	*2.9*				A_1^-	2 398 345.7	*2.6*
$2_{11} \leftarrow 1_{10}$	B_1^-	2 432 731.2	*1.4*	E^-	2 425 944.1	*−0.4*	A_1^-	2 419 758.8	*0.6*
$3_{12} \leftarrow 2_{11}$	A_1^+	2 443 565.2	*0.7*	E^+	2 436 810.3	*3.5*	B_1^+	2 430 649.2	*4.1*
$4_{13} \leftarrow 3_{12}$	B_1^-	2 454 383.8	*1.9*	E^-	2 447 663.8	*4.7*	A_1^-	2 441 536.1	*3.8*
$5_{14} \leftarrow 4_{13}$	A_1^+	2 465 184.1	*2.8*	E^+	2 458 502.0	*2.6*	B_1^+	2 452 419.7	*0.3*
$6_{15} \leftarrow 5_{14}$	B_1^-	2 475 956.8	*−5.1*	E^-	2 469 328.6	*3.4*			
$7_{16} \leftarrow 6_{15}$				E^+	2 480 132.1	*−1.8*			
$3_{13} \leftarrow 4_{14}$	B_1^-	2 367 392.5	*−3.1*	E^-	2 360 644.3	*3.2*		2 354 452.9	*−4.0*
$2_{12} \leftarrow 3_{13}$	A_1^+	2 378 350.6	*−2.4*					2 365 368.9	*−3.8*
$1_{11} \leftarrow 2_{12}$				E^-	2 382 471.7	*−0.2*		2 376 262.7	*−4.3*

TABLE III. (*Continued*.)

Transition		A_1^+, B_1^-	Obs–Calc		E^+, E^-	Obs–Calc		B_1^+, A_1^-	Obs–Calc
$2_{12} \leftarrow 2_{11}$	A_1^+	2 410 795.4	*−3.4*						
$3_{13} \leftarrow 3_{12}$	B_1^-	2 410 584.0	*−2.8*						
$4_{14} \leftarrow 4_{13}$	A_1^+	2 410 301.5	*−2.8*						
$2_{12} \leftarrow 1_{11}$	A_1^+	2 432 594.2	*−1.9*	E^+	2 425 808.1	*−3.3*		2 419 610.4	*−2.3*
$3_{13} \leftarrow 2_{12}$		2 443 326.2	*−4.0*	E^-	2 436 568.1	*−5.6*		2 430 384.0	*−3.1*
$4_{14} \leftarrow 3_{13}$	A_1^+	2 454 021.7	*−2.8*	E^+	2 447 295.4	*−8.3*		2 441 134.3	*−1.0*
$5_{15} \leftarrow 4_{14}$								2 451 856.0	*−0.4*
$6_{16} \leftarrow 5_{15}$	A_1^+	2 475 290.5	*0.0*						
$7_{17} \leftarrow 6_{16}$				E^+	2 479 278.6	*0.9*		2 473 215.3	*0.3*
Transition		A_2^+, B_2^-	Obs–Calc		E^+, E^-	Obs–Calc		B_2^+, A_2^-	Obs–Calc
$5_{14} \leftarrow 6_{15}$				E_2^-	2 475 047.6	*−5.0*	A_2^-	2 477 963.4	*4.7*
$4_{13} \leftarrow 5_{14}$	B_2^-	2 483 938.5	*3.4*	E_2^+	2 486 767.3	*−0.7*	B_2^+	2 489 739.0	*1.0*
$3_{12} \leftarrow 4_{13}$	A_2^+	2 495 447.0	*0.5*	E_2^-	2 498 314.5	*−1.0*	A_2^-	2 501 336.2	*0.8*
$2_{11} \leftarrow 3_{12}$	B_2^-	2 506 804.9	*4.1*	E_2^-	2 509 696.0	*−1.3*	B_2^+	2 512 759.0	*5.0*
$1_{10} \leftarrow 2_{11}$				E_2^-	2 520 909.4	*−5.5*			
$1_{10} \leftarrow 1_{11}$	B_2^-	2 539 842.8	*1.0*	E_2^+	2 542 757.1	*2.2*	B_2^+	2 545 836.7	*−0.9*
$2_{11} \leftarrow 2_{12}$	A_2^+	2 539 647.1	*−0.1*	E_2^-	2 542 548.6	*4.2*	A_2^-	2 545 603.3	*−1.4*
$3_{12} \leftarrow 3_{13}$	B_2^-	2 539 356.9	*0.1*	B_2^+	2 542 227.1	*0.6*	B_2^+	2 545 250.5	*−2.4*
$4_{13} \leftarrow 4_{14}$				E_2^-	2 541 798.6	*−0.1*			
$2_{11} \leftarrow 1_{10}$				E_2^+	2 564 149.5	*3.4*	B_2^+	2 567 201.4	*−4.3*
$3_{12} \leftarrow 2_{11}$	B_2^-	2 571 664.8	*−2.3*	E_2^-	2 574 540.0	*3.3*	A_2^-	2 577 557.1	*−4.8*
$4_{13} \leftarrow 3_{12}$	A_2^+	2 581 925.6	*2.8*	E_2^+	2 584 757.1	*1.8*			
$5_{14} \leftarrow 4_{13}$				E_2^-	2 594 799.0	*1.8*	A_2^-	2 597 713.9	*−1.4*
$6_{15} \leftarrow 5_{14}$	A_2^+	2 601 927.0	*−0.1*						
$7_{16} \leftarrow 6_{15}$	B_2^-	2 611 660.6	*−3.8*						
$5_{15} \leftarrow 6_{16}$				E_2^-	2 475 285.6	*−3.9*			
$4_{14} \leftarrow 5_{15}$	A_2^+	2 483 958.0	*1.4*	E_2^+	2 486 959.0	*−1.1*			
$3_{13} \leftarrow 4_{14}$	B_2^-	2 495 493.2	*−0.4*	E_2^-	2 498 474.6	*−3.5*	B_2^+	2 501 553.2	*−2.0*
$2_{12} \leftarrow 3_{13}$	A_2^+	2 506 874.5	*0.1*	E_2^+	2 509 831.5	*−2.1*			
$1_{11} \leftarrow 2_{12}$				E_2^-	2 521 022.2	*3.2*	B_2^+	2 524 106.7	*−2.3*
$1_{11} \leftarrow 1_{10}$	A_2^+	2 539 683.6	*0.6*	E_2^+	2 542 621.6	*1.2*	A_2^-	2 545 711.2	*1.6*
$2_{12} \leftarrow 2_{11}$	B_2^-	2 539 184.3	*−0.4*	E_2^-	2 542 144.3	*0.4*			
$3_{13} \leftarrow 3_{12}$	A_2^+	2 538 451.4	*0.5*	E_2^+	2 541 433.6	*−1.1*	A_2^-	2 544 511.5	*1.9*
$4_{14} \leftarrow 4_{13}$	B_2^-	2 537 500.2	*2.3*	E_2^-	2 540 500.0	*0.4*			
$5_{15} \leftarrow 5_{14}$				E_2^+	2 539 348.4	*1.1*			
$2_{12} \leftarrow 1_{11}$	A_2^+	2 561 025.4	*1.3*	E_2^+	2 563 985.1	*1.2*	A_2^-	2 567 065.9	*−1.6*
$3_{13} \leftarrow 2_{12}$	B_2^-	2 571 294.9	*−2.3*	E_2^-	2 574 283.4	*1.6*	B_2^+	2 577 361.6	*1.2*
$4_{14} \leftarrow 3_{13}$	A_2^+	2 581 406.7	*−1.5*	E_2^+	2 584 415.3	*4.8*			
$5_{15} \leftarrow 4_{14}$				E_2^-	2 594 378.7	*0.7*			
Transition		A_1^+, B_1^-	Obs–Calc		E^+, E^-	Obs–Calc		B_1^+, A_1^-	Obs–Calc
				$K_a = 0 \rightarrow 1$ *c*-type transitions					
$6_{15} \leftarrow 7_{07}$	B_1^-	2 490 379.4	*−6.8*	E^-	2 483 685.3	*3.0*			
$5_{14} \leftarrow 6_{06}$	A_1^+	2 501 218.0	*2.5*	E^+	2 494 466.8	*2.1*	B_1^+	2 488 366.0	*−2.8*
$4_{13} \leftarrow 5_{05}$	B_1^-	2 512 057.6	*3.8*	E^-	2 505 263.4	*3.0*	A_1^-	2 499 119.6	*2.2*
$3_{12} \leftarrow 4_{04}$	A_1^+	2 522 905.3	*5.6*	E^+	2 516 074.0	*4.1*	B_1^+	2 509 895.1	*3.8*
$2_{11} \leftarrow 3_{03}$	B_1^-	2 533 753.0	*1.0*	E^-	2 526 896.4	*3.1*	A_1^-	2 520 693.5	*4.2*
$1_{10} \leftarrow 2_{02}$	A_1^+	2 544 608.3	*−1.2*	E^+	2 537 733.7	*3.0*	B_1^+	2 531 509.6	*−8.0*
$1_{11} \leftarrow 1_{01}$	B_1^-	2 566 280.9	*−2.2*	E^-	2 559 405.6	*2.2*	A_1^-	2 553 175.9	*−2.3*
$2_{12} \leftarrow 2_{02}$	A_1^+	2 566 178.0	*1.3*	E^+	2 559 316.7	*−0.5*	B_1^+	2 553 097.9	*−1.8*
$3_{13} \leftarrow 3_{03}$	B_1^-	2 566 018.0	*0.6*	E^-	2 559 183.1	*−3.8*	A_1^-	2 552 980.9	*−1.2*
$4_{14} \leftarrow 4_{04}$	A_1^+	2 565 806.1	*0.7*	E^+	2 559 005.4	*−6.3*	B_1^+	2 552 825.4	*−0.3*
$5_{15} \leftarrow 5_{05}$	B_1^-	2 565 542.1	*1.0*	E^-	2 558 783.3	*−7.0*	A_1^-	2 552 630.8	*0.1*
$6_{16} \leftarrow 6_{06}$	A_1^+	2 565 226.6	*1.6*	E^+	2 558 517.4	*−3.9*	B_1^+	2 552 397.5	*−0.1*
$7_{17} \leftarrow 7_{07}$	B_1^-	2 564 859.2	*1.7*	E^-	2 558 212.0	*8.9*	A_1^-	2 552 123.5	*−3.3*
$8_{18} \leftarrow 8_{08}$	A_1^+	2 564 442.2	*2.8*	E^+	2 557 837.0	*2.9*	B_1^+	2 551 825.3	*6.4*
$9_{19} \leftarrow 9_{09}$	B_1^-	2 563 970.3	*−1.0*				A_1^-	2 551 473.5	*−1.1*
$10_{110} \leftarrow 10_{010}$	A_1^+	2 563 449.9	*−4.1*						
$11_{111} \leftarrow 11_{011}$	B_1^-	2 562 891.6	*3.0*						
$1_{10} \leftarrow 0_{00}$	A_1^+	2 577 205.1	*1.4*	E^+	2 570 321.3	*−2.1*	B_1^+	2 564 102.2	*0.4*
$2_{11} \leftarrow 1_{01}$	B_1^-	2 588 074.6	*2.0*	E^-	2 581 209.1	*−2.5*	A_1^-	2 575 010.1	*4.6*
$3_{12} \leftarrow 2_{02}$	A_1^+	2 598 946.6	*4.2*	E^+	2 592 107.4	*−2.1*	B_1^+	2 585 934.7	*6.8*
$4_{13} \leftarrow 3_{03}$	B_1^-	2 609 817.5	*5.0*	E^-	2 603 013.2	*−2.2*	A_1^-	2 596 873.3	*5.0*

TABLE III. (*Continued*.)

Transition		A_1^+, B_1^-	Obs–Calc		E^+, E^-	Obs–Calc		B_1^+, A_1^-	Obs–Calc
$5_{14} \leftarrow 4_{04}$	A_1^+	2 620 686.3	*3.9*	E^+	2 613 928.2	*1.3*	B_1^+	2 607 826.7	*0.6*
$6_{15} \leftarrow 5_{05}$	B_1^-	2 631 545.9	*−5.8*	E^-	2 624 842.2	*0.5*	A_1^-	2 618 790.1	*−10.8*
$7_{16} \leftarrow 6_{06}$				E^+	2 635 755.6	*−1.7*			
$8_{17} \leftarrow 7_{07}$				E^-	2 646 663.8	*−6.9*			
Transition		A_2^+, B_2^-	Obs–Calc		E^+, E^-	Obs–Calc		B_2^+, A_2^-	Obs–Calc
$7_{16} \leftarrow 8_{08}$							A_2^-	2 538 563.5	*0.3*
$6_{15} \leftarrow 7_{07}$	A_2^+	2 544 848.1	*−0.1*	E^+	2 547 591.8	*−0.9*	B_2^+	2 550 508.3	*−1.1*
$5_{14} \leftarrow 6_{06}$	B_2^-	2 556 500.9	*0.8*	E^-	2 559 299.8	*−1.4*	A_2^-	2 562 288.8	*−1.8*
$4_{13} \leftarrow 5_{05}$	A_2^+	2 568 014.4	*−0.4*	E^+	2 570 859.4	*−3.7*	B_2^+	2 573 907.7	*−4.3*
$3_{12} \leftarrow 4_{04}$	B_2^-	2 579 392.7	*−3.2*	E^-	2 582 278.1	*−3.6*	A_2^-	2 585 379.3	*1.6*
$2_{11} \leftarrow 3_{03}$				E^+	2 593 555.2	*−4.6*	B_2^+	2 596 690.5	*−0.5*
$1_{10} \leftarrow 2_{02}$	B_2^-	2 601 766.1	*−0.7*	E^-	2 604 697.8	*−1.6*	A_2^-	2 607 822.2	*2.5*
$1_{11} \leftarrow 1_{01}$	A_2^+			E^+	2 626 352.5	*−0.2*	B_2^+	2 629 516.8	*1.7*
$2_{12} \leftarrow 2_{02}$	B_2^-	2 622 950.4	*−1.2*	E^-	2 625 927.7	*−0.7*	A_2^-	2 629 086.2	*2.4*
$3_{13} \leftarrow 3_{03}$	A_2^+	2 622 295.5	*−0.5*	E^+	2 625 297.0	*−0.3*	B_2^+	2 628 447.3	*0.7*
$4_{14} \leftarrow 4_{04}$	B_2^-	2 621 448.2	*0.9*	E^-	2 624 466.3	*0.5*			
$5_{15} \leftarrow 5_{05}$	A_2^+	2 620 426.6	−0.9	E^+	2 622 238.0	*0.1*			
$6_{16} \leftarrow 6_{06}$				E^-	2 620 865.5	*0.1*			
$1_{10} \leftarrow 0_{00}$				E^-	2 637 292.5	*0.4*			
$2_{11} \leftarrow 1_{01}$				E^+	2 647 878.9	*0.8*	B_2^+	2 651 013.0	*1.8*
$3_{12} \leftarrow 2_{02}$	B_2^-	2 655 434.3	*0.4*	E^-	2 658 322.5	*1.1*	A_2^-	2 661 421.5	*1.5*
$4_{13} \leftarrow 3_{03}$	A_2^+	2 665 771.6	*3.7*	E^+	2 668 620.8	*2.9*	B_2^+	2 671 673.8	*3.4*
$5_{14} \leftarrow 4_{04}$	B_2^-	2 675 959.0	*−1.6*	E^-	2 678 769.0	*5.6*	A_2^-	2 681 759.5	*2.0*
$6_{15} \leftarrow 5_{05}$	A_2^+	2 686 003.0	*−3.8*	E^+	2 688 753.4	*1.1*	B_2^+	2 691 674.4	*−1.0*
$7_{16} \leftarrow 6_{06}$	B_2^-	2 695 903.6	*3.2*	E^-	2 698 576.2	*−2.0*	A_2^-	2 701 417.2	*0.1*
$8_{17} \leftarrow 7_{07}$	A_2^+	2 705 635.7	*1.2*	E^+	2 708 235.1	*0.9*	B_2^+	2 710 978.1	*0.4*
Transition		A_1^+, B_1^-	Obs–Calc		E^+, E^-	Obs–Calc		B_1^+, A_1^-	Obs–Calc
				$K_a = 1 \rightarrow 0$ *c*-type transitions					
$6_{06} \leftarrow 7_{17}$	B_1^-	2 246 929.2	*2.2*						
$5_{05} \leftarrow 6_{16}$	A_1^+	2 258 295.9	*0.1*						
$4_{04} \leftarrow 5_{15}$	B_1^-	2 269 589.1	*−0.3*						
$3_{03} \leftarrow 4_{14}$	A_1^+	2 280 805.4	*0.1*						
$2_{02} \leftarrow 3_{13}$	B_1^-	2 291 941.9	*1.0*				A_1^-	2 286 909.7	*−1.9*
$1_{01} \leftarrow 2_{12}$							B_1^+	2 297 979.2	*−2.5*
$3_{03} \leftarrow 2_{12}$	A_1^+	2 356 969.5	*−1.9*	E_1^+	2 354 509.5	*−1.8*			
$4_{04} \leftarrow 3_{13}$	B_1^-	2 367 506.3	*−1.0*	E^-	2 365 029.8	*−1.1*	A_1^-	2 362 411.1	*−1.3*
$5_{05} \leftarrow 4_{14}$	A_1^+	2 377 959.7	*1.6*	E^+	2 375 461.4	*−0.9*	B_1^+	2 372 819.6	*−2.5*
$6_{06} \leftarrow 5_{15}$				E^-	2 385 806.6	*−0.8*			
$7_{07} \leftarrow 6_{16}$	A_1^+	2 398 608.9	*−2.4*	E_1^+	2 396 068.8	*−0.3*			
Transition		A_2^+, B_2^-	Obs–Calc		E^+, E^-	Obs–Calc		B_2^+, A_2^-	Obs–Calc
$2_{02} \leftarrow 3_{13}$	A_2^+	2 358 494.6	*−1.2*						
$1_{01} \leftarrow 2_{12}$	B_2^-	2 369 536.1	*−1.0*						
$2_{02} \leftarrow 1_{11}$				E^+	2 415 297.9	*1.2*	B_2^+	2 417 288.6	*−1.4*
$3_{03} \leftarrow 2_{12}$	B_2^-	2 423 601.6	*0.8*	E^-	2 425 955.6	*2.4*			
$4_{04} \leftarrow 3_{13}$	A_2^+	2 434 181.2	*2.0*						
$5_{05} \leftarrow 4_{14}$	B_2^-	2 444 676.3	*−1.5*						

frared radiation is emitted from the rotational levels of small vibrationally excited molecular gases which are usually different isotopomers of methanol, CH_2F_2, and N_2H_4.

The far infrared light is directed into a Martin–Puplett polarizing diplexer consisting of two wire mesh polarizers and a Michelson interferometer. The diplexer used to free space couple the fixed FIR light onto an antenna contacting a Ga:As Schottky barrier diode as well as to separate the reradiated sidebands from the unmixed FIR carrier. Four different diodes were used in the collection of these data (1T12, 1T13, 1T15, and 1T24) purchased from Crowe's laboratory at the University of Virginia. Sidebands are generated by mixing the output from a Hewlett–Packard microwave generator with the fixed frequency FIR in the diode. The microwaves are tunable from 2 to 24 GHz and can be doubled and tripled to increase coverage to 60 GHz. This produces sidebands that are equal to the FIR frequency plus and minus the microwave frequency, giving a scanning window of 120 GHz with a 4 GHz gap around the fixed FIR frequency.

After exiting the diplexer, the tunable radiation is then

TABLE IV. 83 cm^{-1} $(D_2O)_2$ band, acceptor wag fitted constants (MHz), 1σ uncertainties in italics.

	A_1^+/B_1^-		E_1^+/E_1^-		B_1^+/A_1^-	
		$K_a=0$				
$(B+C)/2$	5392.987	*0.157*	5395.775	*0.070*	5397.968	*0.106*
D_j	0.0023	*0.004*	0.0113	*0.0007*	0.0142	*0.001*
Band origin	2 477 619.8	*1.1*				
Interchange	3927.7	*2.2*				
Bifurcation	39.1	*1.7*				
	A_2^-/B_2^+		E_2^-/E_2^+		B_2^-/A_2^+	
$(B+C)/2$	5406.826	*0.236*	5406.873	*0.241*	5407.800	*0.235*
D_j	0.0362	*0.002*	0.0383	*0.0022*	0.0365	*0.002*
Band origin	2 477 299.3	*3.4*				
Interchange	3348.5	*6.8*				
Bifurcation	155.1	*6.3*				
Acceptor switch[a]	53 GHz					
$I(g)$[a]	3637		$I(ag)$[a]	291		
	A_1^+/B_1^-		E_1^+/E_1^-		B_1^+/A_1^-	
		$K_a=1$				
$(B+C)/2$	5427.278	*0.079*	5424.624	*0.089*	5419.785	*0.05*
D_j	0.033	*0.001*	0.0494	*0.0013*	0.0326	*5E-04*
$(B-C)/(4+h)$	14.872	*0.029*	13.854	*0.019*	13.896	*0.022*
d_j	−0.0002	*9E−04*	−0.0001	*0.001*	−0.001	*0.002*
Band origin	2 565 200.5	*0.6*				
Interchange	11 939.141	*1.4*				
Bifurcation	−329.416	*1.2*				
	A_2^-/B_2^+		E_2^-/E_2^+		B_2^-/A_2^+	
$(B+C)/2$	5343.400	*0.780*	5344.365	*0.384*	5340.337	*1.573*
D_j	−0.0603	*0.024*	0.0108	*0.007*	−0.0276	*0.138*
$(B-C)/(4+h)$	24.440	*0.485*	18.849	*0.225*	17.146	*1.612*
d_j	−0.1321	*0.021*	−0.0639	*0.0053*	−0.1039	*0.136*
Band origin	2 632 020.4	*4.1*				
Interchange	5023.49	*8.1*				
Bifurcation	−109.97	*5.7*				
Acceptor Switch[a]	120 GHz					
$I(g)$[a]	8481		$I(ag)$[a]	3458		
A rotational constant[a]	126.6 GHz					
σ (std. dev. of fit) ''1's''	1.06	rms error of resid. ''1's''			2.95	
Number of transitions ''1's''	188					
σ (std. dev. of fit) ''2's''	2.76	rms error of resid. ''2's''			2.08	
Number of transitions ''2's''	176					

[a]Constants not fit.

passed through a wire mesh Fabry–Perot etalon to filter the sidebands from the laser carrier radiation and directed into a vacuum chamber pumped by an 1345 l/s roots blower backed by two mechanical pumps. The sidebands enter the vacuum chamber through a hole in one of two mirrors that form a Herriot cell. The sidebands intersect the molecular beam at 90° making 18–22 passes (ca. 2 m path length) and exiting through the same hole.

The transmitted light is then focused onto a detector, and the signal is sent to a lock-in amplifier which demodulates the FM signal using a 2 f detection scheme. Two detectors were available for use in these experiments. Both use a Ga:Ge photoconductor chip, one is mechanically stressed and covers the frequency range 50–110 cm^{-1}, whereas the unstressed chip covers the frequency range 110–150 cm^{-1}.

The sensitivity of the experiment is typically 10^{-6} minimum fractional absorption. The Doppler limited linewidth is about 2 MHz. The accuracy of the line measurement is about 5 MHz and is limited by both the laser drift and noise.

The clusters are produced by bubbling argon or helium with a backing pressure of 10–15 psi through H_2O or D_2O. Clustering is enhanced by using a 4 pulsed slit jet as described in Refs. 29 and 30, and are typically cooled to a rotational temperature of ~5 K. The background pressure in the chamber is 30–34 mTorr (Ar) or 300 mTorr (He). Spectra of the four intermolecular vibrations studied here are shown in Figs. 3, 5, 7, and 10.

III. SPECTRAL ANALYSIS

The spectra are fit to a prolate top Hamiltonian with perturbations to account for the slight asymmetry. The energy level expression[32] is

$$E(J,K_a) = v_0 + (B+C)/2[J(J+1) - K_a^2] - D_j[J(J+1) - K_a^2]^2 + (-1)^{J+K_a+K_c} \times \{(B-C)/4[J(J+1)] - d_j[J(J+1) - K_a^2]^2\}. \quad (1)$$

The band origin is $v_0(B+C)/2$ is the averaged rotational constant for the complex, and D_j is a centrifugal distortion constant. $(B-C)/4$ accounts for the slight asymmetry of the complex and d_j is the asymmetry distortion constant. The asymmetry perturbation breaks the parity degeneracy of the prolate top energy level expression for $|K_a|>0$, shifting one component up and one down. J is a good quantum number and K_a is nearly a good quantum number in this expression, with J being the total angular momentum quantum number of the complex. K_a is the projection of J onto the body-fixed axis. The energy levels can be labeled using the near-prolate scheme that correlates K_a and K_c, so for $J=1$, $|K_a|=1$ there are two energy levels labeled 1_{10} and 1_{11} with the latter being the lowest in energy.

The two components of the acceptor switching splitting refer to the multiplets of three energy levels labeled either $A_1/E/B_1$ or $A_2/E/B_2$ (Fig. 2). Energy levels labeled $A_1/E/B_1$ are called the ''1's'' with E being labeled E_1 when it occurs in the multiplet with A_1 and B_1. Energy levels corresponding to $A_2/E/B_2$ are called the ''2's'' with E labeled E_2 when it occurs as part of the multiplet with A_2 and B_2. Each tunneling component is fit separately, although, when possible the three components associated with a particular multiplet of the ''1's'' or ''2's'' are fit together to estimate the interchange (I) tunneling splitting and the bifurcation (B) shift in the following manner. For $J=0$, $K_a=0$ the expressions used are

$$E(A_1^+/A_2^-) = E(J=0,K_a=0) - I/2, \quad (2)$$

$$E(E_1^+/E_2^-) = E(J=0,K_a=0) + 2B, \quad (3)$$

$$E(B_1^+/B_2^-) = E(J=0,K_a=0) + I/2, \quad (4)$$

where $E(J=0,Ka=0)$ is from Eq. (1).

Each triplet is fit to a band origin wherein the center of the ground state $K_a=0$ triplet is assumed equal to 0. Therefore the difference of the observed band origins for the triplets is the *change* in the acceptor switching splitting between the two states under investigation. In general transitions between multiplets of different labelings, 1 or 2, are forbidden, and it is not possible to directly measure the acceptor switching splitting. However, the selection rules as they are defined do not forbid transitions between the different E states, but these transitions have not yet been observed and are expected to be very weak. Paul *et al.*[33] were able to simultaneously fit the acceptor switching splitting of the ground state and the excited vibrational state acceptor antisymmetric stretch measured in IR cavity ringdown spectroscopy experiments in $(D_2O)_2$, to a cosine function. Using this model the acceptor switching splitting in $K_a''=0$ was found to be 53 GHz (± 1 GHz). For $(D_2O)_2$ the acceptor switching splitting can be determined in the excited vibrational states using this ground state value.

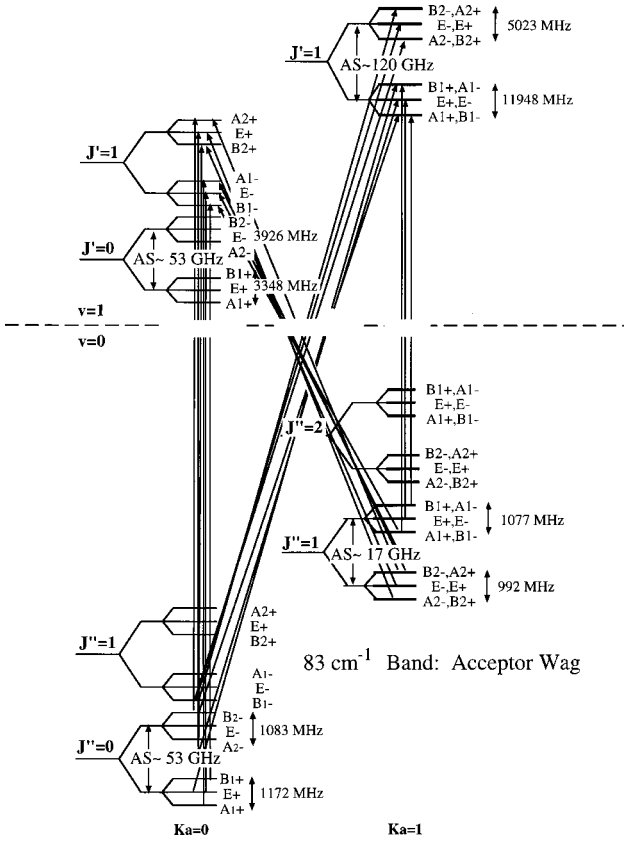

FIG. 6. 83 cm^{-1} $(D_2O)_2$, acceptor wag (ν_8) energy level diagram. $Q(1)$ transitions with $J''=1$ and $R(0)$ transitions with $J''=0$ are shown.

The VRT spectra are fit using a Levenberg–Marquardt nonlinear least squares fitting routine.[34] The residuals for the far-infrared transitions are less than 5 MHz, ca. the absolute accuracy of the spectrometer. Microwave data for the ground state[35,36] are included in the fit to constrain the rotational constants of the ground state. In most cases the residuals for these transitions are 1 MHz or less.

IV. RESULTS AND DISCUSSION

All of the intermolecular vibrations discussed below were measured with the Berkeley terahertz spectrometers. Only the 83 cm^{-1} $(D_2O)_2$ band has been previously reported.[15,16] Additional data for the 83 cm^{-1} band is presented here as well as for three new vibrations at 65 cm^{-1}, 90 cm^{-1}, and 104 cm^{-1}. A re-examination of the ''perturbed states'' of the 83 cm^{-1} band shows that a misassignment was made in that analysis. Corrections were made to the 83 cm^{-1} assignment and a new band centered at 90 cm^{-1} was assigned and fit.

A. The 83 cm^{-1} band: Acceptor wag (ν_8) revisited

Whereas Busarow *et al.*[25] reported a FIR rotation-tunneling spectrum of $(H_2O)_2$ in 1989, the first far infrared vibration–rotation–tunneling spectra of an intermolecular vi-

TABLE V. 65 cm^{-1} $(D_2O)_2$ band: donor torsion (ν_{12}) transition frequencies (MHz). Residuals (observed−calculated values) in italics.

Transition		A_1^+, B_1^-	Obs−Calc		E^+, E^-	Obs−Calc		B_1^+, A_1^-	Obs−Calc
					$K_a = 0 \rightarrow 1$				
$8_{18} \leftarrow 9_{09}$				E^-	1 938 016.7	*−5.8*	A_1^-	1 935 516.6	*−4.2*
$7_{17} \leftarrow 8_{08}$				E^+	1 950 113.0	*−1.5*	B_1^+	1 947 601.2	*−0.2*
$6_{16} \leftarrow 7_{07}$	B_1^-	1 964 590.9	*0.8*	E^-	1 962 061.2	*0.5*	A_1^-	1 959 537.5	*0.8*
$5_{15} \leftarrow 6_{06}$	A_1^+	1 976 398.3	*1.1*	E^+	1 973 859.3	*1.2*	B_1^+	1 971 326.3	*1.8*
$4_{14} \leftarrow 5_{05}$	B_1^-	1 988 051.1	*−0.2*						
$3_{13} \leftarrow 4_{04}$	A_1^+	1 999 550.2	*−0.4*	E^+	1 996 998.2	*1.4*		1 994 448.3	*−0.4*
$2_{12} \leftarrow 3_{03}$	B_1^-	2 010 892.6	*−0.6*	E^-	2 008 333.4	*−0.9*	A_1^-	2 005 781.6	*0.2*
$1_{11} \leftarrow 2_{02}$	A_1^+	2 022 077.4	*−0.5*	E^+	2 019 514.2	*−1.0*	B_1^+	2 016 960.6	*1.4*
$1_{10} \leftarrow 1_{01}$	B_1^-	2 043 866.9	*−0.7*	E^-	2 041 303.1	*−0.1*	A_1^-	2 038 745.2	*−0.7*
$2_{11} \leftarrow 2_{02}$	A_1^+	2 043 665.3	*−1.1*	E^+	2 041 103.9	*0.0*	B_1^+	2 038 547.4	*−0.9*
$3_{12} \leftarrow 3_{03}$	B_1^-	2 043 364.0	*−1.2*	E^-	2 040 804.0	*−1.4*	A_1^-	2 038 251.0	*−1.4*
$4_{13} \leftarrow 4_{04}$	A_1^+	2 042 963.1	*−1.4*	E^+	2 040 406.5	*−1.5*	B_1^+	2 037 857.3	*−1.5*
$5_{14} \leftarrow 5_{05}$	B_1^-	2 042 464.5	*−0.5*	E^-	2 039 911.7	*−0.9*	A_1^-	2 037 367.3	*−1.2*
$6_{15} \leftarrow 6_{06}$	A_1^+	2 041 866.9	*−1.0*	E^+	2 039 319.2	*−0.9*	B_1^+	2 036 781.4	*−1.1*
$7_{16} \leftarrow 7_{07}$	B_1^-	2 041 174.7	*0.4*	E^-	2 038 631.8	*0.0*	A_1^-	2 036 101.8	*−0.2*
$8_{17} \leftarrow 8_{08}$	A_1^+	2 040 384.9	*−0.6*	E^+	2 037 850.3	*0.6*	B_1^+	2 035 329.2	*0.5*
$9_{18} \leftarrow 9_{09}$	B_1^-	2 039 503.4	*0.2*	E^-	2 036 977.3	*1.2*	A_1^-	2 034 464.4	*0.1*
$10_{09} \leftarrow 10_{010}$	A_1^+	2 038 529.2	*0.1*	E^+	2 036 013.7	*−0.4*	B_1^+	2 033 511.5	0.9
$11_{010} \leftarrow 11_{011}$	B_1^-	2 037 466.1	*0.8*						
$1_{11} \leftarrow 0_{00}$				E^+	2 052 107.7	*−0.2*	B_1^+	2 049 549.8	*−0.9*
$2_{12} \leftarrow 1_{01}$	B_1^-	2 065 215.1	*1.3*		2 062 652.6	*0.0*	A_1^-	2 060 098.2	*0.5*
$3_{13} \leftarrow 2_{02}$	A_1^+	2 075 594.5	*1.2*	E^+	2 073 038.1	*1.6*	B_1^+	2 070 487.5	*2.2*
$4_{14} \leftarrow 3_{03}$	B_1^-	2 085 812.0	*1.9*	E^-	2 083 260.5	*1.4*	A_1^-	2 080 711.6	*−1.7*
$5_{15} \leftarrow 4_{04}$	A_1^+	2 095 866.2	*2.1*	E^+	2 093 321.8	*1.4*	B_1^+	2 090 784.2	*2.4*
$6_{16} \leftarrow 5_{05}$	B_1^-	2 105 756.6	*1.0*	E^-	2 103 221.9	*1.7*	A_1^-	2 100 693.1	*2.3*
$7_{17} \leftarrow 6_{06}$	A_1^+	2 115 484.6	*−0.1*	E^+	2 112 960.2	*1.3*	B_1^+	2 110 442.1	*1.2*
$8_{18} \leftarrow 7_{07}$	B_1^-	2 125 051.0	*−0.9*	E^-	2 131 958.5	*2.3*			
$9_{19} \leftarrow 8_{08}$	A_1^+	2 134 456.5	*−1.6*						
Transition		A_2^+, B_2^-	Obs−Calc		E^+, E^-	Obs−Calc		B_2^+, A_2^-	Obs−Calc
					2 007 285.0	*−1.7*			
$6_{16} \leftarrow 7_{07}$	A_2^+	2 013 897.0	*−0.7*	E^+	2 018 165.4	*−3.9*			
$5_{15} \leftarrow 6_{06}$	B_2^-	2 024 753.1	*−2.4*	E^-	2 029 049.0	*−2.0*			
$4_{14} \leftarrow 5_{05}$	A_2^+	2 035 617.7	*3.7*	E^+	2 039 930.5	−0.8	B_2^+	2 044 301.8	*−0.4*
$3_{13} \leftarrow 4_{04}$	B_2^-	2 046 472.1	*−1.6*	E^-	2 050 808.6	*−0.9*	A_2^-	2 055 199.5	*0.4*
$2_{12} \leftarrow 3_{03}$	A_2^+	2 057 334.0	*−1.0*	E^+	2 061 683.6	*−1.7*	B_2^+	2 066 089.6	*0.5*
$1_{11} \leftarrow 2_{02}$				E^-	2 072 557.6	*−0.3*			
$1_{10} \leftarrow 1_{01}$							B_2^+	2 098 662.1	*−0.2*
$2_{11} \leftarrow 2_{02}$	B_2^-	2 089 811.3	*0.7*	E^-	2 094 161.0	*−0.2*	A_2^-	2 098 565.9	*−0.1*
$3_{12} \leftarrow 3_{03}$	A_2^+	2 089 694.1	*−0.7*	E^+	2 094 029.8	*−1.1*	B_2^+	2 098 420.7	*−0.6*
$4_{13} \leftarrow 4_{04}$	B_2^-	2 089 537.6	*−1.5*	E^-	2 093 856.0	*−0.4*	A_2^-	2 098 228.3	*0.1*
$5_{14} \leftarrow 5_{05}$	A_2^+	2 089 341.6	*−0.9*	E^+	2 093 636.7	*−0.7*	B_2^+	2 097 986.6	*0.2*
$6_{15} \leftarrow 6_{6}$	B_2^-	2 089 105.0	*1.4*	E^-	2 093 373.0	*−0.5*	A_2^-	2 097 695.8	*0.1*
$7_{16} \leftarrow 7_{7}$				E^+	2 093 064.0	*−0.3*	B_2^+	2 097 355.5	*−0.1*
$8_{17} \leftarrow 8_{08}$				E^-	2 092 710.2	*0.9*			
$9_{18} \leftarrow 9_{09}$				E^+	2 092 309.1	*0.6*			
$10_{09} \leftarrow 10_{010}$				E^-	2 091 861.3	*−0.4*			
$1_{11} \leftarrow 0_{00}$	B_2^-	2 100 790.3	*0.7*	E^-	2 105 151.1	*0.5*			
$2_{12} \leftarrow 1_{01}$	A_2^+	2 111 651.6	*−0.5*	E^+	2 116 003.2	*−0.4*			
$3_{13} \leftarrow 2_{02}$				E^-	2 126 852.3	*3.2*			
$4_{14} \leftarrow 3_{03}$	A_2^+	2 133 369.6	*2.5*	E^+	2 137 690.7	*4.6*			
$6_{16} \leftarrow 5_{05}$				E^+	2 159 334.0	*5.1*			
$7_{17} \leftarrow 6_{06}$				E^-	2 170 132.1	*0.2*			
Transition		A_1^+, B_1^-	Obs−Calc		E^+, E^-	Obs−Calc		B_1^+, A_1^-	Obs−Calc
					$K_a = 1 \rightarrow 2$				
$2_{20} \leftarrow 2_{11}$	A_1^+	2 177 017.3	*−0.2*	E^+	2 174 742.2	*0.3*	B_1^+	2 172 425.0	*0.1*
$3_{21} \leftarrow 3_{12}$	B_1^-	2 176 840.1	*0.2*	E^-	2 174 569.3	*0.8*	A_1^+	2 172 257.1	*−0.1*
$4_{22} \leftarrow 4_{13}$	A_1^+	2 176 602.5	*−0.6*	E^+	2 174 335.9	*−1.6*	B_1^+	2 172 330.4	*−0.2*
$5_{23} \leftarrow 5_{14}$	B_1^-	2 176 306.6	*−0.7*	E^-	2 174 404.8	*−0.7*	A_1^-	2 171 755.1	*0.6*
$6_{24} \leftarrow 6_{15}$	A_1^+	2 175 951.9	*−0.5*	E^+	2 173 703.4	*−0.6*			
$7_{25} \leftarrow 7_{16}$	B_1^-	2 175 536.6	*−2.1*				A_1^-	2 171 031.5	*0.9*
$8_{26} \leftarrow 8_{17}$	A_1^+	2 175 064.7	*−1.5*						
$2_{20} \leftarrow 1_{11}$	A_1^+	2 198 815.7	*0.9*				A_1^-	2 194 220.7	*−0.1*

TABLE V. (*Continued*.)

Transition		A_1^+, B_1^-	Obs–Calc		E^+, E^-	Obs–Calc		B_1^+, A_1^-	Obs–Calc
$3_{21} \leftarrow 2_{12}$				E^+	2 207 310.1	*−1.5*	B_1^+	2 204 997.8	*−0.5*
$5_{23} \leftarrow 4_{14}$	B_1^-	2 231 033.7	*−0.4*	E^+	2 228 775.9	0.9			
$6_{24} \leftarrow 5_{15}$	A_1^+	2 241 716.3	*1.5*	E^-	2 239 464.4	−0.3	A_1^+	2 237 176.3	*0.1*
$7_{25} \leftarrow 6_{16}$	B_1^-	2 252 368.2	*3.4*	E^+	2 250 128.2	2.6			
$8_{26} \leftarrow 7_{17}$				E^-	2 260 756.1	−1.2			
$2_{21} \leftarrow 2_{12}$	B_1^-	2 177 116.3	*0.0*	E^-	2 174 841.8	0.9	A_1^-	2 172 522.7	*−0.8*
$3_{22} \leftarrow 3_{13}$	A_1^+	2 177 035.6	*−0.4*	E^+	2 174 765.4	0.5	B_1^+	2 172 452.6	*−0.3*
$4_{23} \leftarrow 4_{14}$	B_1^-	2 176 925.8	*−1.2*	E^-	2 174 663.1	1.3	A_1^-	2 172 357.2	*0.4*
$5_{24} \leftarrow 5_{15}$	A_1^+	2 176 787.1	*−0.2*	E^+	2 174 530.8	1.1	B_1^+	2 172 233.4	*−0.3*
$6_{25} \leftarrow 6_{16}$	B_1^-	2 176 613.3	*−1.6*	E^-	2 174 365.0	−1.6	A_1^-	2 172 080.6	*−0.7*
$7_{26} \leftarrow 7_{17}$	A_1^+	2 176 406.5	*−0.5*	E^+	2 174 168.7	−1.4	B_1^+	2 171 895.8	*−1.4*
$8_{27} \leftarrow 8_{18}$							A_1^-	2 171 678.7	*0.3*
$2_{21} \leftarrow 1_{10}$	B_1^-	2 198 782.0	*0.8*				A_1^-	2 194 187.3	*0.0*
$3_{22} \leftarrow 2_{11}$	A_1^+	2 209 481.9	*0.1*	E^+	2 207 208.3	−1.5	B_1^+	2 204 898.4	*1.4*
$5_{24} \leftarrow 4_{13}$	A_1^+	2 230 687.0	*−0.4*	E^+	2 228 428.5	1.3	B_1^+	2 226 132.1	*−0.9*
$6_{25} \leftarrow 5_{14}$	B_1^-	2 241 188.2	*1.5*	E^-	2 238 933.1	−1.6	A_1^-	2 236 648.4	*0.1*
$7_{26} \leftarrow 6_{15}$	A_1^+	2 251 614.5	*1.8*	E^+	2 249 372.3	2.0	B_1^+	2 247 098.1	*0.2*
$8_{27} \leftarrow 7_{16}$				E^-	2 259 730.5	0.2	A_1^-	2 257 473.4	*−0.5*
Transition		A_1^+, B_1^-	Obs–Calc		E^+, E^-	Obs–Calc		B_1^+, A_1^-	Obs–Calc
				$K_a = 1 \rightarrow 0$					
$6_{06} \leftarrow 7_{17}$	A_1^+	2 035 433.3	*2.6*				B_1^+	2 024 788.5	*−1.3*
$5_{05} \leftarrow 6_{16}$	B_1^-	2 045 923.3	*−0.5*						
$4_{04} \leftarrow 5_{15}$	A_1^+	2 056 473.4	*−1.3*	E^+	2 051 059.8	−0.5	B_1^+	2 045 690.9	*−0.7*
$3_{03} \leftarrow 4_{14}$	B_1^-	2 067 083.5	*−1.0*	E^-	2 061 641.8	−2.0	A_1^-	2 056 247.6	*−1.8*
$2_{02} \leftarrow 3_{13}$	A_1^+	2 077 752.9	*−1.1*	E^+	2 072 293.0	−0.8	B_1^+	2 066 878.4	*−1.3*
$1_{01} \leftarrow 2_{12}$	B_1^-	2 088 483.4	*−0.3*	E^-	2 083 009.8	−0.7	A_1^-	2 077 582.3	*−0.7*
$0_{00} \leftarrow 1_{11}$	A_1^+	2 099 273.4	*0.0*	E^+	2 093 792.5	−1.2			
$1_{01} \leftarrow 1_{10}$	B_1^-	2 110 148.2	*−0.5*	E^-	2 104 675.5	0.6	A_1^-	2 099 246.6	*−0.2*
$2_{02} \leftarrow 2_{11}$	A_1^+	2 110 198.7	*−1.2*	E^+	2 104 738.3	−0.3	B_1^+	2 099 324.0	*0.2*
$3_{03} \leftarrow 3_{12}$	B_1^-	2 110 273.9	*−1.7*	E^-	2 104 833.7	0.4	A_1^-	2 099 437.5	*−0.6*
$4_{04} \leftarrow 4_{13}$	A_1^+	2 110 373.8	*−1.0*	E^+	2 104 959.0	1.2	B_1^+	2 099 587.2	*−1.4*
$5_{05} \leftarrow 5_{14}$	B_1^-	2 110 494.4	*−1.3*	E^-	2 105 111.8	0.9	A_1^-	2 099 772.7	*−0.8*
$6_{06} \leftarrow 6_{15}$	A_1^+	2 110 636.2	*−0.1*	E^+	2 105 291.0	0.3	B_1^+	2 099 990.0	*−0.7*
$7_{07} \leftarrow 7_{16}$				E^-	2 105 495.1	0.0	A_1^-	2 100 238.3	*0.7*
$8_{08} \leftarrow 8_{17}$				E^+	2 105 721.4	−0.4	B_1^+	2 100 513.2	*1.9*
$9_{09} \leftarrow 9_{18}$				E^-	2 105 966.8	−1.0			
$10_{010} \leftarrow 10_{19}$				E^+	2 106 231.0	1.0			
$2_{02} \leftarrow 1_{11}$	A_1^+	2 132 002.0	*4.9*						
$3_{03} \leftarrow 2_{12}$				E^-	2 137 579.8	3.5	A_1^-	2 132 184.8	*5.6*
$4_{04} \leftarrow 3_{13}$	A_1^+	2 154 098.9	*3.9*						
$5_{05} \leftarrow 4_{14}$							A_1^-	2 154 500.0	*4.3*
$6_{06} \leftarrow 5_{15}$	A_1^+	2 176 397.9	*−0.9*	E^+	2 171 050.3	−1.1			
$7_{07} \leftarrow 6_{16}$	B_1^-	2 187 619.9	*−0.5*	E^-	2 182 320.8	2.1	A_1^-	2 177 053.7	*−2.2*
$8_{08} \leftarrow 7_{17}$				E^+	2 193 632.6	−2.6	B_1^+	2 188 417.7	*−0.9*
$9_{09} \leftarrow 8_{18}$				E^-	2 204 997.8	0.5			
Transition		A_2^-, B_2^+	Obs–Calc		E_2^-, E_2^+	Obs–Calc		B_2^-, A_2^+	Obs–Calc
$6_{06} \leftarrow 7_{17}$	A_2^-	1 569 793.9	*2.1*	E_2^-	1 573 266.5	*−0.5*			
$5_{05} \leftarrow 6_{16}$	B_2^+	1 580 762.7	*−4.0*	E_2^+	1 584 254.1	*−6.5*			
$3_{03} \leftarrow 4_{14}$	B_2^+	1 602 645.2	*−4.0*	E_2^+	1 606 166.9	*−6.8*	A_2^+	1 609 692.7	*1.7*
$2_{02} \leftarrow 3_{13}$	A_2^-	1 613 558.6	*3.1*	E_2^-	1 617 096.4	*5.6*	B_2^-	1 620 618.8	*−0.2*
$1_{01} \leftarrow 2_{12}$				E_2^+	1 627 980.5	*0.2*	A_2^+	1 631 515.4	*−0.2*
$0_{00} \leftarrow 1_{11}$	A_2^-	1 635 293.0	*−1.2*	E_2^-	1 638 840.1	*−0.8*	B_2^-	1 642 380.4	*0.5*
$1_{01} \leftarrow 1_{10}$	B_2^+	1 646 037.2	*−1.6*	E_2^+	1 649 578.5	*−3.1*	A_2^+	1 653 115.4	*−2.1*
$2_{02} \leftarrow 2_{11}$	A_2^-	1 645 864.9	*−1.5*	E_2^-	1 649 399.1	*−1.8*	B_2^-	1 652 928.1	*−2.2*
$3_{03} \leftarrow 3_{12}$	B_2^+	1 645 609.3	*1.8*	E_2^+	1 649 130.3	*0.2*	A_2^+	1 652 647.3	*−2.0*
$4_{04} \leftarrow 4_{13}$	A_2^-	1 645 265.2	*2.9*	E_2^-	1 648 771.1	*1.9*	B_2^-	1 652 273.1	*−1.3*
$5_{05} \leftarrow 5_{14}$	B_2^+	1 644 827.5	*−2.9*	E_2^+	1 648 321.5	*3.0*	A_2^+	1 651 804.7	*−0.7*
$6_{06} \leftarrow 6_{15}$	A_2^-	1 644 312.5	*0.8*	E_2^-	1 647 780.4	*2.2*	B_2^-	1 651 242.3	*0.3*
$7_{07} \leftarrow 7_{16}$	B_2^+	1 643 704.8	*−1.6*	E_2^+	1 647 148.3	*−0.2*	A_2^+	1 650 584.3	*0.5*
$8_{08} \leftarrow 8_{17}$	A_2^-	1 643 014.8	*1.9*				B_2^-	1 649 830.3	*−0.2*
$9_{09} \leftarrow 9_{18}$	B_2^+	1 642 231.8	*−0.5*						
$2_{02} \leftarrow 1_{11}$				E_2^-	1 671 243.1	*2.0*	B_2^-	1 674 775.3	*4.2*
$3_{03} \leftarrow 2_{12}$	B_2^+	1 678 458.0	*4.8*	E_2^+	1 681 982.2	*4.7*	A_2^+	1 685 499.7	*1.8*

bration for $(D_2O)_2$ were reported by Pugliano *et al.*[15] in 1992. Additional data on that band were published in 1993.[16] Three hundred sixty-three parallel *a*-type and perpendicular *c*-type transitions originating from the ground state $K_a''=0$ levels and terminating in the $K_a'=0$ and 1 levels of an intermolecular vibration were observed and analyzed. This vibration was determined to be of A' symmetry and was assigned to the acceptor wag (ν_8). A K_a dependence in the acceptor switching splitting and the donor–acceptor interchange tunneling splitting were observed and the *A* rotational constant for the state was found to be 122.9 GHz very similar to that of the ground state (125.5 GHz).[36] Finally, it was proposed that the $K_a'=1$ levels associated with the ''2's'' were perturbed by the $K_a'=0$ levels of an unidentified vibration. Reexamination of this region and a revised analysis have revealed a different explanation. Below is a review of the findings from the previous work, additional data corresponding to transitions for $K_a''=1\rightarrow K_a'=0$ and 1 and an explanation of the misassignment made regarding the perturbed states. All of the observed VRT spectra for this vibration are shown in Fig. 5, the measured frequencies are listed in Table III. The fitted constants are given in Table IV and the resultant energy level diagram that is the final product of the experiment and analysis is shown in Fig. 6.

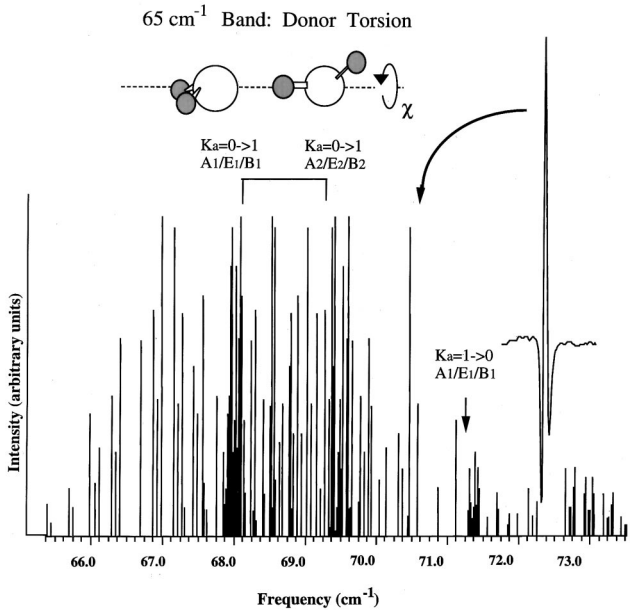

FIG. 7. 65 cm^{-1} $(D_2O)_2$ stick spectrum, donor torsion (ν_{12}). Two hundred forty *b*-type transitions only with $K_a=0\rightarrow1$, $K_a=1\rightarrow0$, $K_a=1\rightarrow2$. Maximum signal-to-noise ~100:1, linewidth ~2 MHz.

1. K_a dependence of tunneling splittings

Only a small (ca. 320 MHz) increase in the acceptor switching splitting is observed for $K_a'=0$ energy levels relative to the ground state, but there is an increase of about 67 GHz for this splitting in the $K_a'=1$ states relative to the ground state $K_a''=0$ and is ~103 GHz larger than the ground state $K_a''=1$ splitting. Recalling the IR cavity ringdown spectroscopy results of Paul *et al.*[33] which provide the first determination of the ground state acceptor switching splitting of 53 GHz for $K_a''=0$, we see that the acceptor switching splitting for this vibration in $K_a'=1$ has more than doubled. It was also observed that the $K_a'=0$ states had the same ordering as the ground state, but the $K_a'=1$ did not. For $K_a'=1$, the ''1's'' are lower than the ''2's,'' i.e., there is an inversion about the acceptor switching splitting. This is the opposite of what is found in the ground state $K_a''=1$.

This large change in the acceptor switching splitting of $K_a'=1$ is attributed to the coupling of the acceptor ''wagging'' vibrational motion to the acceptor switching pathway.[15] Examination of the proposed tunneling pathway shows a flip of the acceptor monomer. This motion is very similar to the acceptor wag vibrational coordinate involving θ_a. Although it is unlikely that the vibrational motion is so simply described by this normal mode, a component of the vibration similar to this normal mode probably couples directly to the acceptor switching pathway.

It has also been proposed that the acceptor switching pathway is altered in the excited state.[15] Note that the end result of acceptor switching is the same as if the acceptor monomer is allowed to rotate 180° about its symmetry axis. In this scenario it is not necessary to rotate the overall complex to return to a symmetrically equivalent structure and the K_a dependence on the ordering is thus removed, viz. the ordering of the levels would be retained from $K_a'=0$ to $K_a'=1$. This would explain the observed energy level ordering. In either case, the high barrier approximation that underlies the local IAM[14,17] treatment of the water dimer does not hold.

Significant changes in the interchange tunneling splitting were also observed to occur upon excitation of the acceptor wag. The interchange splitting in the ground state is fairly constant over the K_a values and symmetry labels with a value of ca. 1 GHz. In the excited state the $K_a'=0$ values are 3.3 and 3.9 GHz for the lower and upper acceptor switching splitting components, respectively. For the $K_a'=1$ state the splitting is significantly increased. It is 11.9 GHz for the ''1's'' and 5.0 GHz for the ''2's.'' While the splittings have significantly increased, the relative ordering remains intact within each fork. The result for the ''2's'' is different here than what was previously reported.[15] The explanation for this is given below.

The geared interchange pathway alone does not explain the differences in the interchange splittings between the ''1's'' and ''2's.'' If it were sufficient, the interchange splittings in each multiplet would be the same. Coudert and Hougen identified the importance of the antigeared interchange pathway in their fit of the dimer data available in 1990 using the local IAM model.[17] They found that the antigeared pathway added to the interchange splitting of the ''1's'' and subtract from the splitting of the ''2's,'' i.e.,

$$\text{for ''1's'':}\quad I(g)+I(ag)=I$$

$$\text{and for ''2's'':}\quad I(g)-I(ag)=I.$$

In $K_a'=0$, $I(g)$ is 3637 MHz and $I(ag)$ is 291 MHz leading to the observed overall interchange splittings. For $K_a'=1$, $I(g)$ is found to be 8481 MHz and $I(ag)$ contribution is 3458 MHz. In the excited state $K_a'=1$ described here, the local IAM model reveals that the antigeared motion is

TABLE VI. 65 cm^{-1} $(D_2O)_2$ band: donor torsion (ν_{12}) fitted constants (in MHz). 1σ uncertainties in italics.

	A_1^+/B_1^-		E_1^+/E_1^-		B_1^+/A_1^-	
			$K_a'=0$			
$(B+C)/2$	5460.37	*0.12*	5457.300	*0.070*	5454.24	*0.151*
D_j	0.0533	*0.0016*	0.0509	*0.0007*	0.051	*0.00029*
Band origin	2 259 943.0	*1.1*				
Interchange	9838.3	*2.2*				
Bifurcation	−50.9	*1.7*				
	A_2^-/B_2^+		E_2^-/E_2^+		B_2^-/A_2^+	
$(B+C)/2$	5402.105	*0.099*	5400.128	*0.167*	5398.756	*0.138*
D_j	0.0374	*0.0011*	0.0365	*0.0031*	0.0375	*0.002*
Band origin	1 733 402.0	*1.1*				
Interchange	6093.3	*2.1*				
Bifurcation	−24.0	*1.9*				
Acceptor switch[a]	474 GHz					
Interchange (g)[a]	7966		Interchange (ag)[a]		1872	
			$K_a'=1$			
$(B+C)/2$	5367.765	*0.0678*	5367.434	*0.066*	5367.022	*0.057*
D_j	0.0274	*0.0007*	0.0291	*0.0007*	0.0282	*0.0005*
$(B-C)/4$	14.831	*0.17*	14.960	*0.014*	15.14	*0.014*
d_j	0		0		0	
Band origin	2 046 774.0	*0.8*				
Interchange	3950.5	*1.7*				
Bifurcation	−3.6	*1.4*				
	A_2^-/B_2^+		E_2^-/E_2^+		B_2^-/A_2^+	
$(B+C)/2$	5422.497	*0.613*	5420.102	*0.179*	5417.918	*0.529*
D_j	0.0465	*0.014*	0.0407	*0.002*	0.0379	*0.0098*
$(B-C)/4$	9.483	*0.091*	9.507	*0.052*	9.535	*0.193*
d_j	−0.0054	*0.0004*	0.0013	*0.0005*	−0.0015	*0.0003*
Band origin	2 099 738.2	*3.7*				
Interchange	7696.9	*7.5*				
Bifurcation	−26.7	*4.9*				
Acceptor switch[a]	106 GHz					
Interchange (g)[a]	5823		Interchange (ag)[a]		1873	
A rotational const.[a]	82 GHz					
σ (std. dev. of fit) ''1's''		0.99	rms error of resid. ''1's''			1.15
σ (std. dev. of fit) ''2's''		1.8	rms error of resid. ''2's''			1.9
Number of trans. ''1's''		240	number of trans. ''2's''			99
	A_1^+/B_1^-		E_1^+/E_1^-		B_1^+/A_1^-	
			$K_a'=2$			
$(B+C)/2$	5412.665	*0.11*	5411.984	*0.114*	5411.38	*0.113*
D_j	0.0433	*0.0017*	0.0437	*0.002*	0.043	*0.0018*
$(B-C)/4$	0.0095	*0.0003*	0.0099	*0.0003*	0.009	*0.0003*
Band origin	2 351 820.3	*1.0*				
Interchange	3520.7	*2.0*				
Bifurcation	−7.0	*1.9*				

[a]These constants were not fit.

more than 40% of the total interchange splitting compared with the ground state where it made up less than 5% for both $(H_2O)_2$ and $(D_2O)_2$ in the IAM description. The bifurcation shift changes by +39 MHz and +157 for the ''1's'' and ''2's,'' respectively in $K_a'=0$, and changes by −329 MHz and −111 MHz in $K_a'=1$ for the ''1's'' and ''2's.''

Pugliano *et al.*[16] postulated that half of the $K_a'=1$ ''2's'' states were perturbed. Q-branches which were believed to belong to this state did not fit well with the observed P- and R-branches, therefore it was hypothesized that the $K_a'=0$ levels of another vibration were perturbing the levels in which the P- and R-branch transitions terminated. These levels correspond to the upper half of the asymmetry splitting. Re-examination of these subbands in light of extensive new data and a better understanding of dimer VRT dynamics reveals an entirely different explanation. A search for the K_a'

$=1 \leftarrow K_a''=1$ transitions was performed, and the corresponding transitions were found for those terminating in the upper half of the asymmetry splitting (those previously believed to be perturbed). However, no transitions were found to terminate in the lower asymmetry component using the rotational constants determined by Pugliano *et al.*[16] New estimates of the $K_a=1 \rightarrow 1$ transitions to the lower asymmetry states were made based on the upper state components. Transitions to these new lower states were then identified. Next, new predictions for the *Q* branches of the $K_a'=1 \leftarrow K_a''=0$ band were made from this fit. Subsequently the correct *Q* branches were identified. The two halves of the asymmetry components can now be fit together. The previously misidentified *Q*-branches actually belong to a separate VRT band centered at 90 cm^{-1}, and coincidentally occurred near the transitions of this vibration in the spectrum. The 90 cm^{-1} band is identified with the acceptor twist vibration and is discussed below.

2. K_a dependence of fitted constants

The energy level expressions used in this fit are not corrected for tunneling contributions to the fitted constants. It can be seen that the fitted constants actually change not only with K_a, but with tunneling component. There is a significant change in the $(B+C)/2$ rotational constant between each of the forks of the acceptor switching splitting, and a smaller variation in $(B+C)/2$ within each fork. In $K_a'=0$, $(B+C)/2$ of the ''1's'' has decreased by an average of 37 MHz (−0.68%) and varies by ±3 MHz within the fork. The $(B+C)/2$ of the ''2's'' decrease by a smaller amount (25 MHz, −0.46%) and vary by ±1.5 MHz. In $K_a'=1$, $(B+C)/2$ of the ''1's'' decreases by only ~8 MHz (−0.16%), but varies by ±5 MHz. The ''2's'' decrease by 91 MHz (1.68%) and varies by ±3 MHz. It has been suggested that $(B+C)/2$ is affected by acceptor switching when the high barrier model breaks down.[17]

The centrifugal distortion constants (D_j) have changed little from the ground state values for the ''1's.'' However, the ''2's'' exhibit very different values from the ground state. Two tunneling states (A_2^-/B_2^+ and B_2^-/A_2^+) have negative D_j's while the E_2^-/E_2^+ states have a positive, but smaller value than the ground state. This suggests that these levels are perturbed. In fact, the $K_a'=0$ ''2's'' states of the new 90 cm^{-1} vibration are believed to be the explicit perturbers. The $K_a'=1$ levels of the acceptor wag are shifted down while the $K_a'=0$ levels of the acceptor twist are shifted up. This will be discussed and described in more detail below.

The asymmetry constants, $(B-C)/4$, were observed to have greatly varying values among the tunneling components in the ground state and are strongly influenced by tunneling.[32] In order to use these for structural information, it is necessary to remove the effects of tunneling. It is easy to rationalize the tunneling influence since $(B-C)/4$ is determined by the position of the light, out-of-plane deuterium atoms. The vibrationally averaged ground state structure corresponds to an acceptor θ_a angle of ~58°; $(B-C)/4$ goes to zero and then switches sign (indicating a change in the *B* and *C* axes) as θ_a goes to 48°. For $K_a'=1$ of the ''1's'' $(B-C)/4$ has increased on average 6 MHz (73%) from ca 8.2 MHz in the ground state $K_a''=1$ with only a 1 MHz variation among tunneling components. For the ''2's'' it has increased by 4 MHz (27%) from ca. 14.9 MHz in the ground state $K_a''=1$ but varies by ±5 MHz among tunneling components.

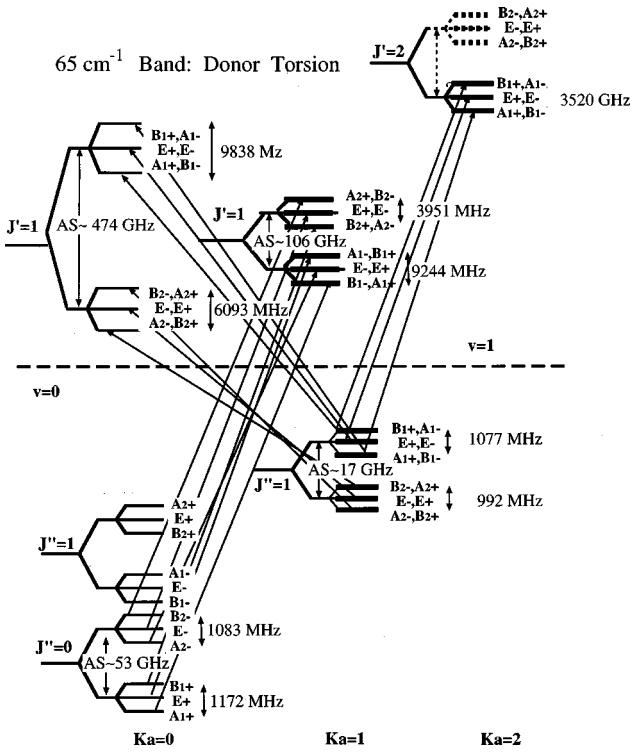

FIG. 8. 65 cm^{-1} $(D_2O)_2$, donor torsion (ν_{12}) energy level diagram. $J=0 \rightarrow 1$, $K_a=0 \rightarrow 1$, $J=1 \rightarrow 1$, $K_a=1 \rightarrow 0$, and $J=1 \rightarrow 2$, $K_a=1 \rightarrow 2$ transitions are shown.

Finally, a new *A* rotation constant was determined for the ν_8 excited state using the relationship

$$(\upsilon^{\text{``1''}}{}_{Ka'=0}+\upsilon^{\text{``2''}}{}_{Ka'=0})/2+A-B = (\upsilon^{\text{``1''}}{}_{Ka'=1}+\upsilon^{\text{``2''}}{}_{Ka'=1})/2, \quad (5)$$

where *B* is average rotational constant and υ's are the band origins for the ''1's'' or ''2's'' for each K_a. The value of *A* was determined to be 122 GHz, ca. 3.5 GHz (<2.8%) decrease below the ground state value of 125.5 GHz.[36] This is reasonable as we do not expect *A* to change much in the acceptor wag vibration.

B. The 65 cm^{-1} band: Donor torsion (ν_{12})

Two hundred forty perpendicular, *b*-type transitions from $K_a''=0$ and 1 of the ground state to $K_a'=0$, 1, and 2 of the excited state have been observed near 65 cm^{-1}. The 240 measured transitions for 15 subbands were fit to an A'' symmetry vibration and assigned to the donor torsion (ν_{12}). The data are listed in Table V and the stick spectrum is shown in Fig. 7. Combination differences for the ground state were used to assign the *J*, K_a, and K_c values of the spectra, as well as to determine the overall symmetry of the vibration. The nuclear spin statistics, which govern relative intensities, allowed the tunneling labels for each subband to be identified.

TABLE VII. 90 cm^{-1} $(D_2O)_2$ band: acceptor twist transition frequencies (MHz). Residuals (observed–calculated values) in italics.

Transition		A_1^+, B_1^-	Obs–Calc		E^+, E^-	Obs–Calc		B_1^+, A_1^-	Obs–Calc
					$K_a = 1 \rightarrow 0$				
$7_{07} \leftarrow 8_{18}$				E^-	2 546 989.0	*−2.1*			
$6_{06} \leftarrow 7_{17}$	A_1^+	2 549 987.5	*−0.6*	E^+	2 556 902.1	*1.8*			
$5_{05} \leftarrow 6_{16}$	B_1^-	2 560 016.4	*−0.7*	E^-	2 566 944.1	*0.5*	A_1^-	2 573 965.1	*−2.5*
$4_{04} \leftarrow 5_{15}$	A_1^+	2 570 179.7	*−3.3*	E^+	2 577 121.8	*0.5*	B_1^+	2 584 161.6	*0.5*
$3_{03} \leftarrow 4_{14}$	B_1^-	2 580 491.0	*5.0*				A_1^-	2 594 483.9	*−0.9*
$2_{02} \leftarrow 3_{13}$				E^+	2 597 882.6	*1.6*	B_1^+	2 604 937.0	*−2.6*
$1_{01} \leftarrow 2_{12}$	B_1^-	2 601 504.6	*1.8*	E^-	2 608 460.2	*−2.5*	A_1^-	2 615 526.1	*0.0*
$0_{00} \leftarrow 1_{11}$				E^+	2 619 177.0	*−1.5*			
$1_{01} \leftarrow 1_{10}$	B_1^-	2 623 165.5	*−1.1*	E^-	2 630 127.2	*0.0*	A_1^-	2 637 192.9	*1.9*
$2_{02} \leftarrow 2_{11}$	A_1^+	2 623 369.6	*−0.4*	E^+	2 630 325.9	*0.1*	B_1^+	2 637 386.2	*0.7*
$3_{03} \leftarrow 3_{12}$	B_1^-	2 623 674.1	*−0.6*	E^-	2 630 623.3	*0.0*	A_1^-	2 637 675.8	*−0.2*
$4_{04} \leftarrow 4_{13}$	A_1^+	2 624 079.6	*−0.4*	E^+	2 631 018.8	*0.0*	B_1^+	2 638 060.8	*−0.4*
$5_{05} \leftarrow 5_{14}$	B_1^-	2 624 584.7	*−0.4*	E^-	2 631 511.5	*−0.1*	A_1^-	2 638 538.8	*−0.6*
$6_{06} \leftarrow 6_{15}$	A_1^+	2 625 188.5	*−0.5*	E^+	2 632 100.6	*0.1*			
$7_{07} \leftarrow 7_{16}$	B_1^-	2 625 892.1	*1.5*	E^-	2 632 784.2	*0.1*			
$8_{08} \leftarrow 8_{17}$	A_1^+	2 626 688.5	*0.1*	E^+	2 633 560.3	*−0.7*			
$9_{09} \leftarrow 9_{18}$	B_1^-	2 627 583.3	*2.4*	E^-	2 634 429.7	*0.3*			
$10_{010} \leftarrow 10_{19}$	A_1^+	2 628 564.9	*−1.4*	E^+	2 635.387.7	*0.5*			
$11_{011} \leftarrow 11_{110}$	B_1^-	2 629 642.3	*−0.3*						
$2_{02} \leftarrow 1_{11}$				E^+	2 652 124.1	*1.2*	B_1^+	2 659 181.4	*−1.3*
$3_{03} \leftarrow 2_{12}$	B_1^-	2 656 415.9	*0.1*				A_1^-	2 670 421.4	*2.0*
$4_{04} \leftarrow 3_{13}$				E^+	2 674 739.8	*1.4*	B_1^+	2 681 782.2	*0.7*
$5_{05} \leftarrow 4_{14}$	B_1^-	2 679 305.4	*−1.9*				A_1^-	2 693 269.0	*2.7*
$6_{06} \leftarrow 5_{15}$	A_1^+	2 690 944.6	*−0.7*	E^+	2 697 861.1	*−0.1*			
$7_{07} \leftarrow 6_{16}$	B_1^-	2 702 710.0	*1.2*	E^-	2 709 606.7	*−1.0*			

Transition		A_2^-, B_2^+	Obs–Calc		B_2^-, A_2^+	Obs–Calc
$7_{07} \leftarrow 8_{18}$	B_2^+	2 496 227.8				
$6_{06} \leftarrow 7_{17}$	A_2^-	2 506 037.6				
$5_{05} \leftarrow 6_{16}$	B_2^+	2 515 988.0		A_2^+	2 504 059.8	
$4_{04} \leftarrow 5_{15}$	A_2^-	2 526 080.8		B_2^-	2 514 054.2	
$3_{03} \leftarrow 4_{14}$	B_2^+			A_2^+	2 524 199.5	
$2_{02} \leftarrow 3_{13}$	A_2^-	2 546 714.6		B_2^-	2 534 512.7	
$1_{01} \leftarrow 2_{12}$	B_2^+	2 557 252.7		A_2^+	2 544 990.2	
$0_{00} \leftarrow 1_{11}$				B_2^-	2 555 634.8	
$1_{01} \leftarrow 1_{10}$	B_2^+	2 578 845.9		A_2^+	2 566 585.0	
$2_{02} \leftarrow 2_{11}$	A_2^-	2 579 028.8		B_2^-	2 566 824.7	
$3_{03} \leftarrow 3_{12}$	B_2^+	2 578 283.7		A_2^+	2 567 156.0	
$4_{04} \leftarrow 4_{13}$				B_2^-	2 567 595.5	
$5_{05} \leftarrow 5_{14}$	B_2^+	2 580.050.8		A_2^+	2 568 119.4	
$6_{06} \leftarrow 6_{15}$	A_2^-	2 580 558.3				
$7_{07} \leftarrow 7_{16}$	B_2^+	2 581 136.0				
$8_{08} \leftarrow 8_{17}$	A_2^-	2 581 788.1				
$2_{02} \leftarrow 1_{11}$	B_2^+	2 600 868.4				
$3_{03} \leftarrow 2_{12}$				A_2^+	2 600 008.3	
$4_{04} \leftarrow 3_{13}$	A_2^-	2 623 535.9		B_2^-	2 611 507.3	
$5_{05} \leftarrow 4_{14}$	B_2^+	2 535 084.0		A_2^+	2 623 155.0	

1. $K_a = 0 \rightarrow 1$ subbands

All six possible VRT subbands corresponding to $K_a = 0 \rightarrow 1$ were observed for the 65 cm^{-1} vibration. The presence of $Q(1)$ and the absence of $P(1)$ verify this assignment. The ''1's'' were fit to a band origin of 2 046 773.9 MHz and the ''2's'' to 2 099 738.3 MHz. All fitted parameters are in Table VI. The difference between the band origins gives the change in the acceptor switching splitting as approximately 53 GHz. Recall that the acceptor switching splitting in the ground state $K_a = 0$ was determined to be 53 GHz, this gives an acceptor switching splitting of 106 GHz in $K_a' = 1$, a factor of 2 larger than the ground state $K_a' = 0$ and more than five times larger than in $K_a'' = 1$. An energy level diagram for this vibration is given in Fig. 8.

The excited state interchange splitting is 3950 MHz for $K_a' = 1$ (more than three times the ground state values) for the ''1's'' and 7697 MHz for the ''2's'' (ca. seven times the ground state values). The interchange splittings can be dissected into the geared and antigeared components which are found to be 5824 MHz and −1874 MHz, respectively. The antigeared motion is now about 32% of the total interchange splitting compared to 5% in the ground state. The bifurcation

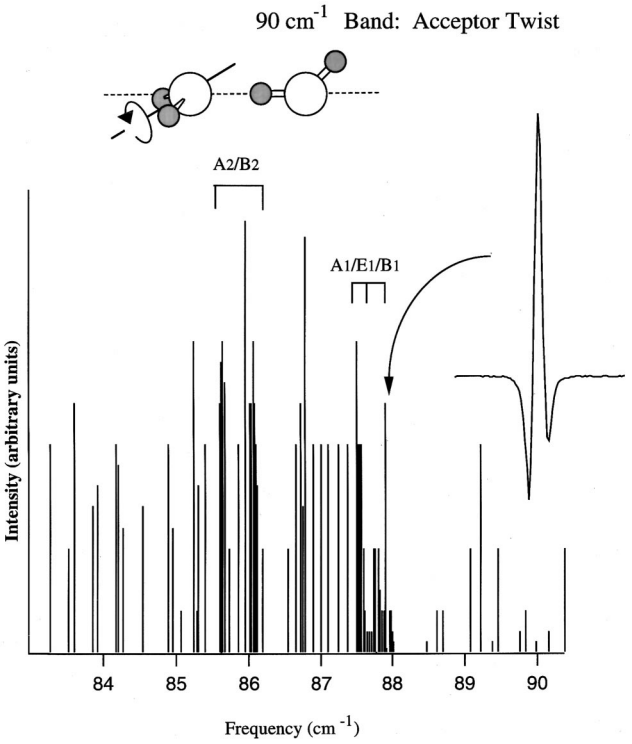

FIG. 9. 90 cm^{-1} $(D_2O)_2$ stick spectrum, acceptor twist (ν_{11}). Eighty-three *b*-type transitions with $K_a=1\rightarrow0$ observed. Maximum signal-to-noise ~50:1, linewidth ~2 MHz. One tunneling component of the ''2's'' is missing.

shift is approximately −3 MHz for the ''1's'' and −27 MHz for the ''2's'' compared to ~0 MHz for the ground state $K_a''=0$ values.

The rotational constants $(B+C)/2$ for the ''1's'' have decreased by 65 MHz (−1.2%) from the ground state $K_a''=0$. The rotational constants within the multiplet do not vary by more than 0.7 MHz. The centrifugal distortion constants (D_j) have decreased by as much as 10 kHz (28%). The asymmetry constants, $(B-C)/4$, are ~15 MHz, almost double the ground state $K_a'=1$ values, and vary with tunneling component by ±0.3 MHz.

In comparison the rotational constants $(B+C)/2$ for the ''2's'' have decreased by only ~12 MHz (<1%), but show a larger variation (up to 4.5 MHz) within the tunneling components of the fork. The centrifugal distortion constants (D_j) have *increased* for the ''2's'' by as much as 9 kHz (25%). The asymmetry constants, $(B-C)/4$, are ~9.5 MHz. A decrease of ~5.5 MHz (36%) from the ''2's'' of the ground state $K_a''=1$.

2. $K_a=1\rightarrow0$ subbands

Transitions corresponding to all six tunneling components have been observed with $K_a=1\rightarrow0$. The observed transitions were verified to be $K_a=1\rightarrow0$, by the presence of $J=1\rightarrow0$ transitions, the fact that the *Q*-branches originated from the *J*, $K_a=1$, $K_c=J-1$ levels, and that there were no transitions corresponding to *Q*-branches originating from the *J*, $K_a=1$, $K_c=J$ levels. The band origin for the ''1's'' was determined to be 2 259 943.0 GHz, more than 213 GHz above the $K_a'=1$ levels of the same symmetry. The band origin for the ''2's'' is 1 733 402.0 MHz resulting in an acceptor switching splitting of 474 GHz, nine times the ground state $K_a''=0$ value.

The interchange splitting for the ''1's'' was determined to be 9838 MHz in $K_a'=0$, and for the ''2's,'' it is 6093 MHz. The geared contribution is 7966 MHz (81%) and the antigeared is 1872 MHz (19%) of the total interchange splitting. The bifurcation shift is ca. −51 MHz for the ''1's,'' and the ''2's'' exhibit a bifurcation shift of −24 MHz compared to 0 MHz for $K_a'=0$ states.

The rotational constants, $(B+C)/2$, for the ''1's'' have increased by an average of 25 MHz (0.46%) from the ground

TABLE VIII. $(D_2O)_2$ 90 cm^{-1} band: acceptor twist (ν_{11}) fitted constants (MHz). 1σ uncertainties in italics.

	A_1^+/B_1^-		E_1^+/E_1^-		B_1^+/A_1^-	
$(B+C)/2$	5491.913	*0.156*	5491.006	*0.163*	5490.073	*0.859*
D_j	0.0438	*0.0012*	0.0457	*0.0016*	0.0527	*0.0250*
Band origin	2 785 356.7	*3.4*				
Interchange	12 952.4	*6.7*				
Bifurcation	−79.8	*3.5*				
number of transitions		55				
σ (standard deviation of fit)		1.49	rms error of residuals		1.04	
	A_2^-/B_2^+[a]		E_2^-/E_2^+		B_2^-/A_2^+[b]	
$(B+C)/2$	5488				5504	
D_j	0.058				0.165	
Band origin	2 656 351					
Interchange	13 286					
Bifurcation	−79					
number off transitions		30				
Acceptor switch[a]		76 GHz				

[a]This constant was not fit.
[b]The constants for these states are assumed to be the correct symmetry. Until the third component is found this assignment is tentative.

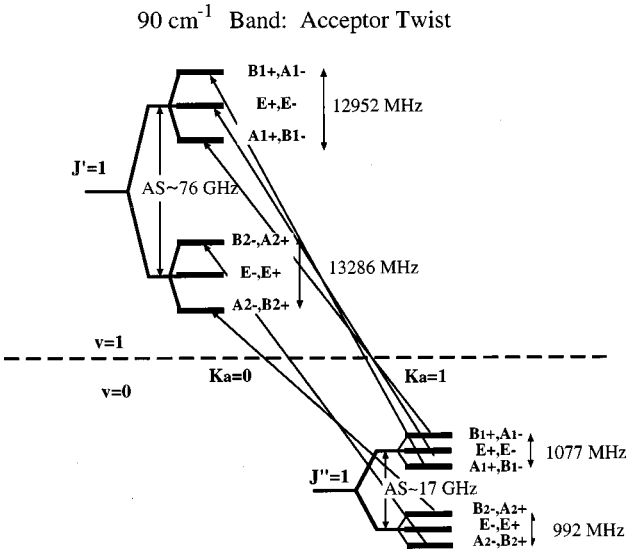

FIG. 10. 90 cm^{-1} $(D_2O)_2$ band, acceptor twist (ν_{11}) energy level diagram. $J=1\rightarrow1$, $K_a=1\rightarrow0$ transitions are shown.

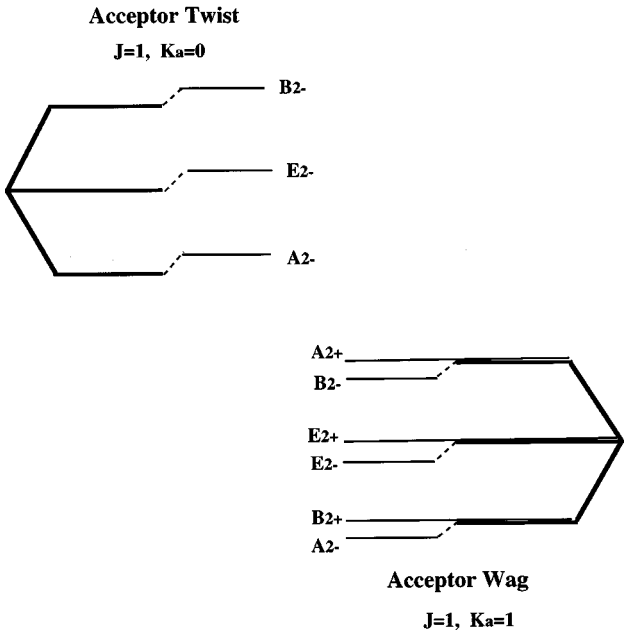

FIG. 11. Perturbation of $K_a'=1$ $A_2/E_2/B_2$ levels of the acceptor wag by the $K_a'=0$ $A_2/E_2/B_2$ levels of the acceptor twist in $(D_2O)_2$.

state and varies by as much as 6 MHz between tunneling components within the fork. The centrifugal distortion constant (D_j) has increased by ~14 kHz (38%).

For the ''2's'' the rotational constants have *decreased* by an average of 32 MHz (0.59%). The variation among tunneling components is less than 4 MHz. The distortion constants (D_j) are very close to the ground state values. The average is ca. 37 kHz compared to 36 kHz for $K_a''=0$.

An A rotational constant was calculated using Eq. (5). A was determined to be 82 GHz, 43 GHz (−34%) less than the ground state value using this method. An A rotational constant of 82 GHz is very unlikely. It is more likely the case that the use of Eq. (5) for determining A is not valid here, or that there is an as yet unobserved perturbation which has shifted the observed band origins. In either case, the 82 GHz value for the A rotational constant should be regarded with skepticism.

3. $K_a=1\rightarrow2$ subbands

Transitions with $K_a=1\rightarrow2$ corresponding to the ''1's'' were observed, but not for the ''2's.'' The absences of $Q(1)$'s and $R(0)$'s as well as the complete absence of P-branch transitions led to these K_a assignments. P-branch transitions would require K_c to change by 2. It was also noted that there are transitions originating from both of the asymmetry components of $K_a''=1$. The interchange splitting was determined to be 3520 MHz and the bifurcation shift has decreased by 7 MHz. An energy level diagram for the excited vibrational state is shown in Fig. 8. The dashed energy levels represent the relative positions where the unobserved transitions are expected to terminate.

The rotational constants $(B+C)/2$ have decreased by an average of 20 MHz (0.37%) and vary only about 1.3 MHz between tunneling components within the fork. The distortion constants (D_j) have increased to 43 kHz from 34 kHz (24%) in the ground state $K_a''=2$ and show little variation among the tunneling components of this fork. The asymmetry parameter, $(B-C)/4$, is ~0.009 MHz compared to 0.002 MHz in the $K_a''=2$.

There are three possible A'' vibrations for the water dimer, the donor torsion (ν_{12}), the acceptor twist (ν_{11}), and the out-of-plane bend (ν_{10}). This A'' vibration was assigned to the donor torsion (ν_{12}), because the out-of-plane bend (ν_{10}) is predicted to be the highest energy intermolecular vibration and most likely out of the range of our spectrometer and the acceptor twist (ν_{11}) vibrational motion has similarities with the interchange tunneling coordinate, therefore, the interchange splitting is expected to be relatively large in this vibration in comparison to the ground state and the other excited states. The A'' vibration at 90 cm^{-1} exhibits this property and was assigned accordingly. The donor torsion is expected to have similarities with the acceptor switching and the bifurcation tunneling pathways, and it is predicted to be the lowest energy intermolecular vibration of the dimer. It mainly involves the χ angle, which is the dihedral angle between the molecular symmetry axes of the constituent monomers. It is not expected that this, or in fact, that any of the intermolecular vibrations will be very harmonic. Most likely there will be coupling of the large amplitude tunneling motions to the intermolecular vibrations, particularly those involving the same molecular coordinates. The acceptor switching splitting has doubled in $K_a'=1$ of this band from $K_a''=0$, and $K_a'=0$ is about nine times larger than $K_a''=0$. The interchange splittings have also increased, but it may be more useful to look at the geared and antigeared components. The geared component is more than five times larger and the antigeared component is more than 30 times larger than the ground state indicating that a significant amount of energy being put into these tunneling coordinates. The antigeared motion is relatively less hindered now, as shown by the large increase in its percentage of the total interchange

TABLE IX. 104 cm^{-1} $(D_2O)_2$ band: in-plane bend transition frequencies (MHz). Residuals (observed–calculated) in italics.

Transition		A_1^+, B_1^-	Obs–Calc		E_1^+, E_1^-	Obs–Calc		$B_1^+ A_1^-$	Obs–Calc
				$K_a=0\rightarrow 0$					
$7_{07}\leftarrow 8_{08}$				E_1^+	3 039 114.0	*−0.88*	B_1^+	3 050 423.1	*−1.83*
$6_{06}\leftarrow 7_{07}$	B_1^-	3 037 585.2	*−4.52*	E_1^-	3 049 787.7	*−2.83*	A_1^-	3 061 254.5	*1.30*
$5_{05}\leftarrow 6_{06}$	A_1^+	3 048 145.9	*−2.89*		3 060 496.2	*1.25*	B_1^+	3 072 090.6	*1.28*
$4_{04}\leftarrow 5_{05}$	B_1^-	3 058 757.4	*−0.66*	E_1^-	3 071 229.6	*2.18*	A_1^-	3 082 930.4	*−2.03*
$3_{03}\leftarrow 4_{04}$	A_1^+	3 069 418.6	*0.47*	E_1^+	3 081 986.8	*−0.56*	B_1^+	3 093 782.0	*0.34*
$2_{02}\leftarrow 3_{03}$	B_1^-	3 080 128.8	*−0.56*	E_1^-	3 092 772.8	*−1.49*			
$1_{01}\leftarrow 2_{02}$	A_1^+	3 090 890.2	*−1.68*				B_1^+	3 115 494.2	*−0.79*
$0_{00}\leftarrow 1_{01}$	B_1^-	3 101 705.6	*0.14*	E_1^-	3 114 426.0	*−0.99*	A_1^-	3 126 355.8	*−1.55*
$1_{01}\leftarrow 0_{00}$	A_1^+	3 123 483.6	*0.24*		3 136 181.6	*1.24*	B_1^+	3 148 088.5	*−0.61*
$2_{02}\leftarrow 1_{01}$	B_1^-	3 134 447.2	*1.60*	E_1^-	3 147 092.9	*0.31*	A_1^-	3 158 956.9	*0.14*
$3_{03}\leftarrow 2_{02}$	A_1^+	3 145 455.1	*0.36*	E_1^+	3 158 027.2	*0.17*	B_1^+	3 169 827.6	*3.19*
$4_{04}\leftarrow 3_{03}$	B_1^-	3 156 509.3	*0.36*	E_1^-	3 168 979.6	*−2.77*	A_1^-	3 180 693.6	*2.41*
$5_{05}\leftarrow 4_{04}$	A_1^-	3 167 609.2	*3.12*		3 179 961.6	*4.41*			
$6_{06}\leftarrow 5_{05}$	B_1^-	3 178 747.6	*3.80*				A_1^-	3 202 416.0	*−2.63*
$7_{07}\leftarrow 6_{06}$				E_1^+	3 201 958.8	*−0.51*	B_1^+	3 213 276.8	*−0.71*
$8_{08}\leftarrow 7_{07}$	B_1^-	3 201 130.8	*0.00*	E_1^-	3 212 983.5	*−0.18*	A_1^-	3 224 133.2	*1.19*
$9_{09}\leftarrow 8_{08}$	A_1^+	3 212 375.2	*0.40*	E_1^+	3 224 022.5	*0.68*	B_1^+	3 234 981.5	*0.29*
$10_{010}\leftarrow 9_{09}$	B_1^-	3 223 648.8	*−0.18*						

splitting. The interchange pathways involve θ_a, ϕ_a, θ_d, and ϕ_d. A modified version of the vibrational motion can be envisioned in which the motion in the χ angle is coupled with a slight twisting in the acceptor ϕ_a angle and flip in the θ_a angle to compensate for the increased repulsion as the free hydrogen on the donor is rotated. This motion begins to look like the geared interchange tunneling and acceptor switching pathways.

All of the fitted rotation parameters show a dependence on K_a and tunneling component, indicating a contamination of these constants with tunneling effects which cannot be removed with this fitting model. The high barrier model is drastically less appropriate for these vibrationally excited states as the tops of the tunneling barriers are approached.

C. The 90 cm^{-1} band: Acceptor twist (ν_{11})

Eighty-three perpendicular, *b*-type transitions corresponding to an A'' vibration have been observed around 90 cm^{-1} with $K_a=0\rightarrow 1$. The *Q* branches of the upper half of the acceptor switching splitting corresponding to the ''1's'' were previously identified as belonging to the 83 cm^{-1} band with $K_a=0\rightarrow 1$ and tunneling labels of ''2's.'' They were misidentified due to their coincidental location in the spectrum. The *P* and *R* branches for each *Q* branch were identified using combination differences. The presence of $P(1)$'s and the fact that the *Q*-branches originate from the *J*, $K_a=1$, $K_c=J-1$ levels were used as verification of the K_a assignments. The transitions are listed in Table VII and a stick spectrum is given in Fig. 9. The fitted constants are summarized in Table VIII, and the energy level diagram can be found in Fig. 10.

$K_a=1\rightarrow 0$ *subbands*. The band origin of the ''1's'' is at 2 785 356.7 MHz (92.8 cm^{-1}). The fitted constants in Table VII show an increase in the $(B+C)/2$ rotational constants for these subbands to an average of 5491 MHz with a variation of ± 1 MHz within the fork. The distortion constants (D_j) have increased slightly to 46.0 kHz (25%). A 12-fold increase in the interchange splitting to a value of 12 952 MHz was determined. A smaller decrease of −79 MHz for the bifurcation shift was estimated.

Using the knowledge that $K_a=0$ ''2's'' are expected to be lower in energy than the $K_a=0$ ''1's'' for A'' vibrations, the ''2's'' were located near 2656 GHz. At this time only two of the three tunneling components have been found and fit. It is believed that the third component has transitions lying in frequency gaps where the sensitivity of the spectrometer was too low, making a search for combination differences impossible. An initial attempt at fitting the observed data lead to the assignment of the two observed tunneling components as belonging to B_2^-/A_2^+ and A_2^-/B_2^+ states. Without reliable intensity measurements it is difficult if not impossible to distinguish between the three tunneling components of the ''2's'' because the combination differences are essentially the same with the accuracy of our measurements. If the above assignment is used, a band origin of 2656 GHz is determined, just 24 GHz above the 83 cm^{-1} $K_a'=1$ levels of the ''2's.'' These tunneling labels were chosen because they give an estimated interchange splitting of ~13 GHz, close to the value of the ''1's.'' If one of these components is chosen to belong to E_2^-/E_2^+ states then the interchange splitting will be on the order of 25 GHz. Using 2656 GHz as the band origin of the ''2's,'' an estimated acceptor switching splitting for $K_a'=0$ of 76 GHz is determined. These assignments will remain tentative until the third component is found and fit. Using Eq. (2) the average band origin for the ''1's'' and ''2's'' with $K_a=0\rightarrow 1$ is predicted to be near 2840 GHz.

It was mentioned previously that the 83 cm^{-1} $K_a'=1$ ''2's'' appeared to be perturbed. It is now believed that the $K_a'=0$ ''2's'' of this 90 cm^{-1} band is the explicit perturber. The fitted constants, particularly the distortion constants (D_j) appear too large for these subbands. The perturbation is

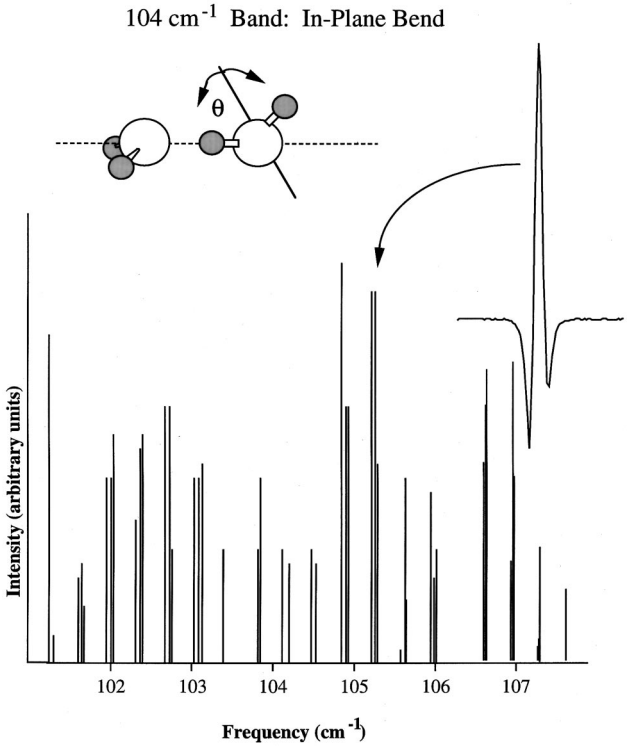

FIG. 12. 104 cm^{-1} $(D_2O)_2$ stick spectrum, in-plane bend (ν_6). Forty-five *a*-type transitions with $K_a=0\rightarrow0$ observed. Maximum signal-to-noise ~50:1, linewidth ~2 MHz.

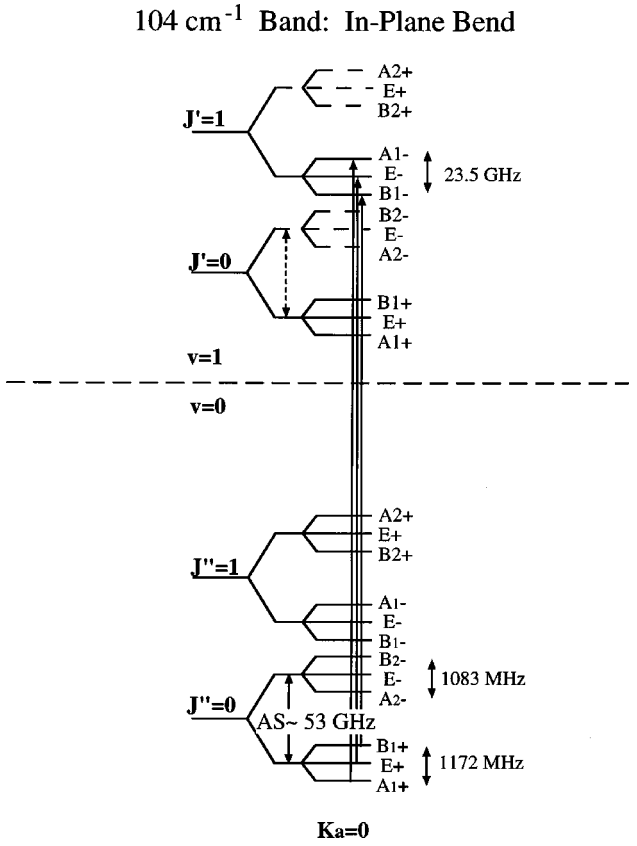

FIG. 13. 104 cm^{-1} $(D_2O)_2$, in-plane bend (ν_6) energy level diagram. $J=0\rightarrow1$, $K_a=0\rightarrow0$ *a*-type transitions are shown.

relatively small compared to a similar situation occurring in the ground state of the $(H_2O)_2$ which has a Coriolis interaction between $K_a=0$ and 1 states of the ''2's.'' This is most likely due to the fact that the two vibrations are of different symmetry, but it is possible to get interactions between individual tunneling components of the same overall symmetry, same *J*, and with $\Delta K_a=\pm1$. In this interaction the $K_a'=0$ states of this excited vibration interact with the lower asymmetry component of the $K_a'=1$ acceptor wag states. The result is that the $K_a'=0$ levels are pushed up and the $K_a'=1$ levels are pushed down (see Fig. 11). Since all three components of the ''2's'' in the 90 cm^{-1} vibration have not been identified it is not possible to fit a perturbation to these states. An attempt was made at incorporating a Coriolis coupling constant between two of the states. This resulted in an estimate of a Coriolis constant of about 800–1000 MHz. If a value of 1000 MHz is used, the distortion constants in each state resemble those of the corresponding ''1's'' and a slightly better $(B-C)/4$ value for the 83 cm^{-1} states result. This is only meant to be an estimate of the perturbation, as the exact coupling mechanism is probably not the same as the one in the ground state of $(H_2O)_2$. A rigorous treatment of the Coriolis coupling most likely requires the use of higher order terms.

This vibration has been assigned to the A'', acceptor twist (ν_{11}) vibration, which is predicted to be close in energy to the acceptor wag. The acceptor twist normal mode involves a rotation of the acceptor monomer about its symmetry axis involving the acceptor ϕ_a angle. Imagining this motion, it can be seen that it has a component similar to both the geared and antigeared donor–acceptor interchange tunneling pathways previously described. It is also not difficult to

TABLE X. 104 cm^{-1} $(D_2O)_2$ band: in-plane bend (ν_6) fitted constants (MHz). 1σ uncertainties in italics.

	A_1^+/B_1^-		E_1^+/E_1^-		B_1^+/A_1^-	
			$K_a=0$			
$(B+C)/2$	5456.993	*0.218*	5444.517	*0.130*	5433.453	*0.123*
D_j	0.0507	*0.0054*	0.0416	*0.0015*	0.0365	*0.0014*
Band origin	3 124 895.9	*1.4*				
Interchange	23 480.7	*2.8*				
Bifurcation	395.5	*2.5*				
Number of transitions		45				
σ (standard deviation of fit)		1.3	rms errors off residuals			1.01

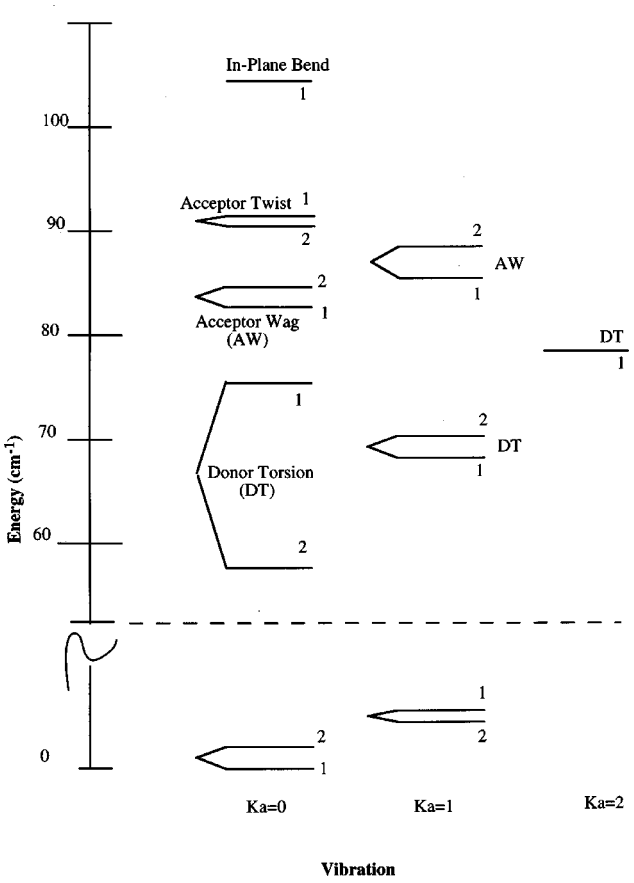

FIG. 14. Summary of observed $(D_2O)_2$ intermolecular vibrations.

imagine that there would be a slight compensating bend of the donor θ_d angle which would draw the oxygen atoms closer together. Both of these ideas would explain the increases observed in the rotational constants and the interchange splitting.

D. The 104 cm^{-1} band: In-plane bend (ν_6)

An A' symmetry vibration was observed near 104 cm^{-1}. Forty-five parallel *a*-type transitions were measured for the three tunneling components of the ''1's'' with $K_a''=0\rightarrow K_a'=0$ but not for the ''2's.'' The data are summarized in Table IX and the stick spectrum is presented in Fig. 12. An interchange splitting of 23 GHz was determined as shown in the energy level diagram of Fig. 13.

$K_a=0\rightarrow 0$. The band origin was determined to be 3 124 895.9 MHz. The K_a assignments were verified by combination differences and the absence of *Q* branches. From the fitted constants in Table X it is observed that the $(B+C)/2$ rotational constants have increased for these subbands to an average of 5445 MHz (0.2%), and vary by ± 12 MHz with tunneling component. This variation is much larger than those appearing in other vibrations. The centrifugal distortion constants (D_J) have also increased. Note, however, that the constants for the B_1^+/A_1^- subband are very close to the values of the ground state.

The interchange splitting is found to be 23 480 MHz (ca, 20 times larger than the ground state), by far the largest increase observed for any $(D_2O)_2$ vibration (see Fig. 13). The bifurcation shift has increased by almost 400 MHz over the ground state $K_a''=0$ value of 0 MHz. If this vibration has a component similar to the interchange tunneling motion this would account for the large increase in the interchange splitting. The large variation in $(B+C)/2$ may suggest it is also affected by the interchange motion, at least for this vibration.

Due to the fact that the $K_a'=0$ ''2's'' have not been observed, an estimate of the acceptor switching splitting cannot be made nor can the interchange splitting be dissected into its geared and anti-geared components. They are expected to be at a higher frequency since this is an A' vibration. Continuous scanning of D_2O clusters has not been performed in the frequency range of 108–137 cm^{-1}. Future work in this frequency range should yield additional $(D_2O)_2$ data.

There are three possible assignments for an A' vibration. The acceptor wag (ν_8) can immediately be eliminated since the 83 cm^{-1} band has been given that assignment. The O–O stretch is expected to occur near 140 cm^{-1}. The final possibility is the donor in-plane bend. While harmonic approximations predict that this vibration is much higher in energy due to the fact that it strains the hydrogen bond, coupling to another vibrational mode by the IPS would make it possible to observe this at a much lower frequency. The normal mode picture of the donor in-plane bend shows a change in the donor θ_d angle. A compensating change in the acceptor θ_a angle, which is similar to the acceptor wag vibration, would not be implausible. This would lead to a coupling between the two vibrations and lowering the energy of the donor in-plane bend in a manner similar to that suggested by Loeser[11] for $(NH_3)_2$. The donor torsion and acceptor twist of $(NH_3)_2$ are believed to be coupled. Coupling is also expected between the vibrational coordinate, the interchange coordinate and the acceptor switching coordinate.

The final piece of evidence that supports this vibrational assignment is the observation that the $(B+C)/2$ rotational constants increase slightly from the ground state. Although the rotational constants are observed to vary with K_a and tunneling component, it is expected that the $(B+C)/2$ values of the O–O stretch will decrease from those of the ground state regardless of K_a and tunneling component. An increase in the separation of the heavy oxygen atoms should result in a decrease in $(B+C)/2$. If the picture of a compensating change in the acceptor θ_a angle with the change is the donor θ_d angle is correct, a decrease in the O–O separation would be possible due to lessened steric hindrances. This would result in a slightly increased $(B+C)/2$ value as observed. Until additional transitions in this band are observed and the data collection near 137 cm^{-1} is completed, this assignment and analysis must remain tentative.

V. SUMMARY

Extensive VRT spectra characterizing four different intermolecular vibrations of $(D_2O)_2$ have been measured and analyzed. Corrections to the previously published vibration observed near 83 cm^{-1} were given along with the assignment of the perturbing vibration centered at 90 cm^{-1}. Additionally, data on the 65 cm^{-1} vibration and the 104 cm^{-1}

vibration were presented. All of these vibrations are both qualitatively and quantitatively different from the predictions of popular pair potentials and represent a significant advance in the understanding of the water dimer intermolecular dynamics. A summary energy level diagram of the measured intermolecular vibrations is given in Fig. 14. These data were used in the recent determination of the water dimer intermolecular potential energy surface by Fellers and Saykally.[37]

[1] R. S. Fellers *et al.*, J. Chem. Phys. **110**, 6306 (1999), and references therein.
[2] R. S. Fellers, Ph.D. thesis, University of California at Berkeley, 1998, and references therein. (http://www.cchem.berkeley.edu/~rjsgrp)
[3] R. S. Fellers *et al.*, Science **284**, 945 (1999).
[4] M. P. Hodges, A. J. Stone, and S. S. Xantheas, J. Phys. Chem. A **101**, 9163 (1997).
[5] R. C. Cohen and R. J. Saykally, J. Chem. Phys. **98**, 6007 (1993), and references therein.
[6] C. A. Schmuttenmaer, R. C. Cohen, and R. J. Saykally, J. Chem. Phys. **101**, 146 (1994), and references therein.
[7] M. J. Elrod and R. J. Saykally, J. Chem. Phys. **103**, 933 (1995), and references therein.
[8] E. H. T. Olthof, A. van der Avoird, and P. E. S. Wormer, J. Chem. Phys. **101**, 8430 (1994).
[9] T. R. Dyke and J. S. Muenter, J. Chem. Phys. **60**, 2929 (1974).
[10] T. R. Dyke, J. Chem. Phys. **66**, 492 (1977).
[11] J. G. Loeser, Ph.D. thesis, University of California at Berkeley, 1995, and references therein.
[12] T. R. Dyke, K. M. Mack, and J. S. Muenter, J. Chem. Phys. **66**, 498 (1977).
[13] J. T. Hougen, J. Mol. Spectrosc. **114**, 395 (1985).
[14] L. H. Coudert and J. T. Hougen, J. Mol. Spectrosc. **130**, 86 (1988).
[15] N. Pugliano and R. J. Saykally, J. Chem. Phys. **96**, 1832 (1992).
[16] N. Pugliano, J. D. Cruzan, J. G. Loeser, and R. J. Saykally, J. Chem. Phys. **98**, 6600 (1993).
[17] L. H. Coudert and J. T. Hougen, J. Mol. Spectrosc. **139**, 259 (1990).
[18] D. J. Wales, Adv. Mol. Vib. Collision Dynamics **3**, 365 (1998).
[19] J. R. Reimer and R. O. Watts, Chem. Phys. **85**, 83 (1984).
[20] J. R. Reimer, R. O. Watts, and M. L. Klein, Chem. Phys. **64**, 95 (1982).
[21] N. Pugliano and R. J. Saykally, Science **257**, 1937 (1992).
[22] J. D. Cruzan *et al.*, Science **271**, 59 (1996).
[23] K. Liu, M. G. Brown, J. D. Cruzan, and R. J. Saykally, Science **271**, 62 (1996).
[24] K. Liu *et al.*, Nature (London) **381**, 501 (1996).
[25] K. L. Busarow *et al.*, J. Chem. Phys. **90**, 3937 (1989).
[26] G. A. Blake *et al.*, Rev. Sci. Instrum. **62**, 1701 (1991).
[27] K. B. Laughlin, Ph.D. thesis, University of California at Berkeley, 1988.
[28] D. W. Steyert, Ph.D. thesis, University of California at Berkeley, 1991.
[29] K. Liu *et al.*, Rev. Sci. Instrum. **67**, 410 (1996).
[30] K. Liu, Ph.D. thesis, University of California at Berkeley, 1996.
[31] M. G. Brown, Ph.D. thesis, University of California at Berkeley, 1999.
[32] G. T. Fraser, R. D. Suenram, and L. H. Coudert, J. Chem. Phys. **90**, 6077 (1989).
[33] J. P. Paul, R. A. Provencal, and R. J. Saykally, J. Phys. Chem. A **102**, 3279 (1998).
[34] *Numerical Recipes in FORTRAN*, 2nd ed., edited by W. H. Press, S. A. Teukolsky, W. T. Vetterling, and B. P. Flannery (Cambridge University Press, New York, 1992), p. 675.
[35] E. Zwart, J. J. ter Meuen, W. L. Meerts, and L. H. Coudert, J. Mol. Spectrosc. **147**, 27 (1991).
[36] E. Meerts, J. J. ter Meulen, and W. L. Meerts, Chem. Phys. Lett. **173**, 115 (1990).
[37] R. S. Fellers and R. J. Saykally (in preparation).